A projectile for a rectangular barreled rail gun

Juanche, Francisco M.

Monterey, California. Naval Postgraduate School

NAVAL POSTGRADUATE SCHOOL
Monterey, California

THESIS

A PROJECTILE FOR
A RECTANGULAR BARRELED RAIL GUN

by

Francisco M. Juanche

December 1999

Thesis Advisor: Conrad F. Newberry
Co-Advisor: William B. Maier II

Approved for public release; distribution is unlimited.

REPORT DOCUMENTATION PAGE

Form Approved OMB No. 0704-0188

1. AGENCY USE ONLY *(Leave blank)*	2. REPORT DATE	3. REPORT TYPE AND DATES COVERED
	December 1999	Master's Thesis

4. TITLE AND SUBTITLE
A PROJECTILE FOR A RECTANGULAR BARRELED RAIL GUN

5. FUNDING NUMBERS

6. AUTHOR(S)
Juanche, Francisco M.

7. PERFORMING ORGANIZATION NAME(S) AND ADDRESS(ES)
Naval Postgraduate School
Monterey, CA 93943-5000

8. PERFORMING ORGANIZATION REPORT NUMBER

9. SPONSORING / MONITORING AGENCY NAME(S) AND ADDRESS(ES)

10. SPONSORING / MONITORING AGENCY REPORT NUMBER

11. SUPPLEMENTARY NOTES
The views expressed in this thesis are those of the author and do not reflect the official policy or position of the Department of Defense or the U.S. Government.

12a. DISTRIBUTION / AVAILABILITY STATEMENT
Approved for public release; distribution is unlimited.

12b. DISTRIBUTION CODE

13. ABSTRACT *(maximum 200 words)*

The Physics Department at the Naval Postgraduate School is developing a concept to overcome the problems that keep present rail guns from being practical weapons. The rails must be replaced often if the rail gun operation is to be continuous. Replacing the rails in present rail gun configurations is time consuming. The Physics Department's design concept uses a rectangular barrel as part of the solution to the problem of replacing the rails. The projectile will require flat surfaces to maintain electrical contact with the flat rails and aerodynamic stabilization because of the lack of angular momentum. This thesis develops one possible model of a projectile for a rectangular barreled rail gun, which could be used to replace the standard five-inch gun found on most warships. The proposed projectile is successfully modeled as a five inch projectile with flat areas planed onto opposite sides and long chord, short span fins attached in a cruciform configuration. The computer programs used to develop the projectile model are included to allow evaluation of alternate configurations.

14. SUBJECT TERMS	15. NUMBER OF PAGES
Projectiles, Rail Guns, Computer Modeling	98
	16. PRICE CODE

17. SECURITY CLASSIFICATION OF REPORT	18. SECURITY CLASSIFICATION OF THIS PAGE	19. SECURITY CLASSIFI- CATION OF ABSTRACT	20. LIMITATION OF ABSTRACT
Unclassified	Unclassified	Unclassified	UL

NSN 7540-01-280-5500

Standard Form 298 (Rev. 2-89)
Prescribed by ANSI Std. 239-18

Approved for public release; distribution is unlimited

A PROJECTILE FOR A RECTANGULAR BARRELED RAIL GUN

Francisco M. Juanche
Lieutenant Commander, United States Navy
B.A., San Francisco State University, 1987

Submitted in partial fulfillment of the
requirements for the degree of

MASTER OF SCIENCE IN APPLIED PHYSICS

from the

NAVAL POSTGRADUATE SCHOOL
December 1999

Author: [redacted]

Francisco M. Juanche

Approved by: [redacted]

Conrad F. Newberry, Advisor

[redacted]

William B. Maier II, Co-Advisor

[redacted]

William B. Maier II, Chairman
Department of Physics

ABSTRACT

The Physics Department at the Naval Postgraduate School is developing a concept to overcome the problems that keep present rail guns from being practical weapons. The rails must be replaced often if the rail gun operation is to be continuous. Replacing the rails in present rail gun configurations is time consuming. The Physics Department's design concept uses a rectangular barrel as part of the solution to the problem of replacing the rails. The projectile will require flat surfaces to maintain electrical contact with the flat rails and aerodynamic stabilization because of the lack of angular momentum. This thesis develops one possible model of a projectile for a rectangular barreled rail gun, which could be used to replace the standard five-inch gun found on most warships. The proposed projectile is successfully modeled as a five inch projectile with flat areas planed onto opposite sides and long chord, short span fins attached in a cruciform configuration. The computer programs used to develop the projectile model are included to allow evaluation of alternate configurations.

TABLE OF CONTENTS

LIST OF SYMBOLS

AR	aspect ratio
β	aerodynamic quantity that appears in many formulas, $(M^2 - 1)^{1/2}$
b	span of single fin
CD	total drag force
C_{DF}	form drag
C_{Df}	skin friction drag
C_F	form drag coefficient
C_{Fb}	form drag coefficient for nose/body combination
C_{Ff}	form drag coefficient for fins
C_f	skin friction drag coefficient
C_{fb}	skin friction drag coefficient for nose/body combination
C_{ff}	skin friction drag coefficient for fins
C_{fb}'	skin friction drag coefficient for nose/body combination modified for equations of motion
C_{ff}'	skin friction drag coefficient for fins combination modified for equations of motion
CG	center of gravity
$CN_{\alpha f}$	normal force coefficient for fins
$CN_{\alpha n}$	normal force coefficient for nose/body combination
C_{ma}	mean aerodynamic chord
C_r	root chord
C_t	tip chord
c_p	specific heat at constant pressure
d	diameter of projectile
dt	time step
f	fineness ratio, ose length divided by maximum projectile diameter
f_{cf}	compressible flow factor
γ	ratio of specific heats, 1.4 for air
g	gravity
H_{ba}	height of base area
h	width of electrical contact area
I_b	first moment of body
I_{ep}	first moment of end plate
I_f	first moment of fins
I_n	first moment of nose
in	inches
K_{BW}, k_{BW}	interference factors for body in the presence of fins
K_{WB}, k_{WB}	interference factors for fins in the presence of body
k	modified drag for equations of motion
kg	kilograms
Λ	sweep angle of fin's leading edge
L	length of nose
L_b	length of projectile's body
L_{bs}	length of projectile's body with shaved sides

L_{bw}	length of projectile's body with wedge insert
L_T	length of total projectile
μ	coefficient of kinematic viscosity or Mach angle, determined by context
M	Mach number
m	mass or meters, determined by context
m_b	mass of projectile's body
m_e	mass of explosive
m_f	mass of fin
m_n	mass of nose
$NV_{o/s}$	volume of ogive nose with shaved sides
$NV_{o/w}$	volume of ogive nose with wedge insert
$NV_{s/s}$	volume of spherical nose with shaved sides
$NV_{s/w}$	volume of spherical nose with wedge insert
%	user entered percentage of total body length for root chord
ϕ	angle of fire
p	pressure
Q	heat (in BTUs in equation (2.1))
q	dynamic head
ρ,ρ_a	ambient air density
ρ_c	density of casing material
ρ_e	density of explosive compound
ρ_0,ρ_{0a}	air density at sea level
Re	Reynold's number
Re_f	Reynold's number for fins
$Re_{n/b}$	Reynold's number for nose/body combination
R_f	radius of curvature of biconvex fins
R_n	radius of curvature of projectile's nose (in inches in equation (2.1))
RV	volume removed from nose by planing flat sides on to the projectile
r	radius of projectile
r'	maximum height of area removed by planing flat sides on to the projectile
r_{ba}	radius of base area
σ	semivertex angle of reference cone for ogive nose
S	total surface area
S_{ba}	base area
S_{bs}	surface area of body with shaved sides
S_{bw}	surface area of body with wedge insert
S_{cs}	cross sectional area
S_{csw}	cross sectional area of projectile with wedge insert
S_{css}	cross sectional area of projectile with shaved sides
S_d	planform area of delta wing if fins were not clipped
S_{ecs}	cross sectional area of explosive
S_{effs}	fin surface area effected by Mach cones
S_f	planform area of fin
$S_{no/s}$	surface area of ogive nose with shaved sides
$S_{no/w}$	surface area of ogive nose with wedge insert
$S_{ns/s}$	surface area of spherical nose with shaved sides

$S_{ns/w}$	surface area of spherical nose with wedge insert
S_{pcs}	cross sectional area of projectile
S_o	surface area of an ogive nose
S_{wf}	wetted area of fins
s	seconds
st	skin thickness
τ	thickness ratio, maximum fin thickness divided by chord
θ	angle subtended by arc length
θ_{ba}	angle subtended by arc of curved section of base
θ_f	angle subtended by arc of biconvex fin
T	temperature
T_0	temperature at sea level
V_f	volume of fin
v	velocity
v0	initial velocity
v_t	terminal velocity
v_x	lateral velocity
v_y	vertical velocity
X_{CPf}	position of center of pressure for fins
X_{CPfb}	position of center of pressure for interference of nose/body and fins
X_{CPn}	position of center of pressure for nose/body combination
x	lateral position, i.e. range
y	vertical position, i.e. altitude

I. INTRODUCTION

This thesis models an aerodynamically stable projectile for a rectangular barreled rail gun. The three computer programs used in modeling this projectile are provided so that the models can be updated to meet changing requirements.

The first section of Chapters II and III present the reasoning and assumptions for the selections made from the available alternatives regarding that chapter's subject. The second section of Chapters II and III develop the equations used in the computer model associated with that chapter. Chapter IV uses the assumptions from the previous two chapters and begins with four sections of equation development. The final section of each chapter analyzes the output of the computer program developed in the previous sections from that chapter.

This thesis is multidisciplinary, with advisors in both the Aeronautical Engineering Department and in the Physics Department. Readers from different disciplines are reminded that they may find more detail relating to their particular subject area than they feel necessary, but readers from other disciplines may need that detail to understand what is being done.

A. BACKGROUND

A rail gun uses the interaction between electrical currents and magnetic fields to accelerate a projectile. The rails in a rail gun are electrically charged with the projectile completing the electrical circuit between them. An electric current flows through the rails and projectile creating a magnetic field. The magnetic field interacts with the flowing electrons, which accelerates the projectile out of the barrel. The acceleration is

increased as the magnetic field is increased. The magnetic field increase as the electric current increases.

The Physics Department at the Naval Postgraduate School has a rail quick change concept for a rail gun. The large electrical current used in rail guns to achieve the large accelerations to attain large muzzle velocities in present rail gun designs also vaporizes some of the surface of the projectile. The vaporized material settles on the rails, fouling the barrel in about five firings or less. The rails must be removed for cleaning before the rail gun can be fired again. Present rail gun designs take thirty minutes of longer to remove and replace the rails, assuming clean replacement rails are available. Conventionally fired guns can maintain a rate of fire of several shots per minute for extended periods. A thirty-minute cease-fire between five shot salvoes is not an acceptable rate of fire for a rail gun weapon system.

The Naval Postgraduate School Physics Department's rail gun design concept, among other things, will shorten the time required to replace the rails and thus increase the firing rate in comparison with existing rail gun designs. The computer models developed in this thesis provide graphs for the analysis of the aerodynamic effects imposed upon a projectile by this alternate design as physical dimensions are changed. The resultant projectile performance can also be analyzed. Only those details of the rail gun design effecting the design of the projectile, such as barrel shape, will be discussed here. Rail gun design is such a broad field of study that all other details of the concept, such as power requirements and building techniques. Are left to other investigators.

The most important feature of the new rail gun concept is its rectangular barrel. The projectile, in common with all rail gun projectiles, requires an electrical contact

surface capable of withstanding the immense electrical currents used in rail guns. The magnitude of these electrical currents depends on the weight of the projectile, the desired muzzle velocity, and the length of the barrel. The electrical contact surfaces of the new design's rectangular barrel will be flat rails on opposite sides of the barrel. Therefore, to maintain good electrical contact the electrical contact surface on the projectile will have to be flat. The rectangular barrel, having no rifling, will not impart the rotation that provides the angular momentum that usually keeps projectiles stable in flight. The lack of angular momentum adds the requirement of some form of aerodynamic stabilization for the projectile.

B. BASIC THEORY

A variety of aerodynamic theories, presented by S. S. Chin [Ref. 1] and by William Pitts, Jack Nielsen, and George Kaattari [Ref. 2], were used in development of the computer models used herein to compare projectile shapes and related performance. Slender body and nose/body theories from Reference (1) were used to determine the skin friction drag, form drag, boattail drag, and base drag of the body of the projectile. Airfoil theory, also from Reference (1), was used for analyzing small fins added to the projectile. Figure (1) on the next page shows these stabilizing fins attached to the projectile body. These fins compensate for the lack of spin stabilization normally provided by the angular momentum caused by the rotation of the projectile. The fins, however, also add drag. Wing/body interference factors from Reference (2) were used in the equations that combine the aerodynamic characteristics of the projectile body and fins to provide a total drag coefficient for the equations of motion and the aerodynamic coefficients for the stability study of the complete projectile.

Figure (1) Projectile Schematic

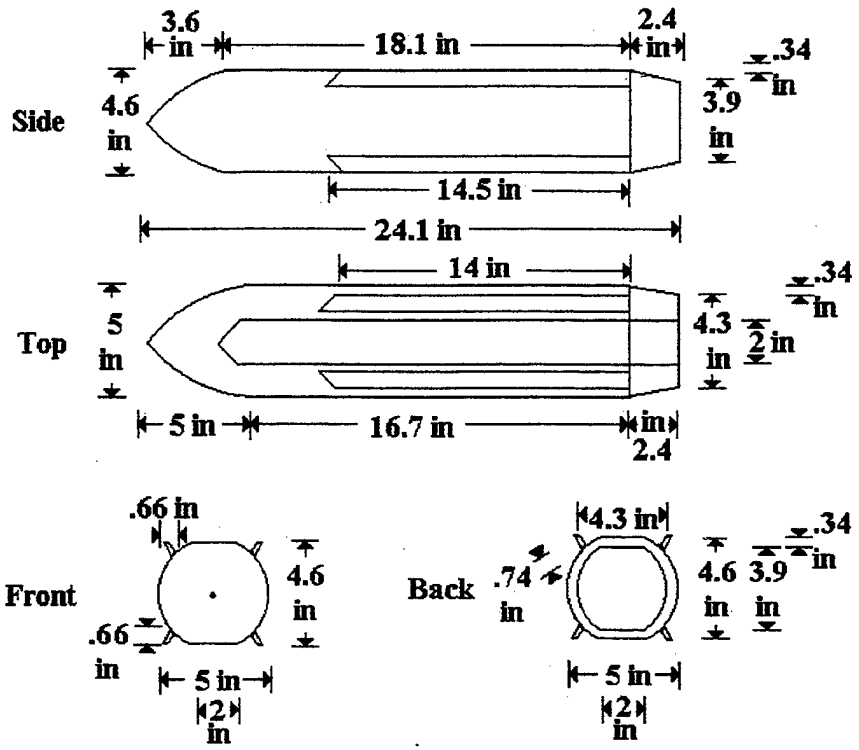

Numerical integration theory is required for the computer model that calculates projectile trajectory and impact energy. As a projectile travels through space, many factors interact. At any point in time the velocity is changing due to the effects of drag, which in turn changes the distance the projectile will have traveled at the next point in time and the velocity it has when it gets there. To further complicate matters, the drag itself changes with the velocity and with the air density, which is changing with the vertical position of the projectile. With so many interactions between variables a closed solution to the integration of the equations of motion is difficult, consequently numerical integration schemes are required to solve the equations of motion. The Euler-Cromer method was selected for the numerical integration of the equations of motion because of its stability in long calculations. The Euler-Cromer method, occasionally referred to as the last point method, uses a loop, shown in simplified form in Figure (2) as a flow chart.

The program loop takes the final position of the projectile from the previous time step and calculates the velocity at that point and then uses that velocity to calculate the next point in the projectile's trajectory. The accuracy of the integration for most numerical integration methods is increased as the time steps are made smaller, but the round-off error often increases with each calculation. The Euler-Cromer method is stable in long calculations because the round-off errors tend to cancel each other so the calculation does not diverge.

Figure (2) Euler Cromer Numerical Integration Flow Chart

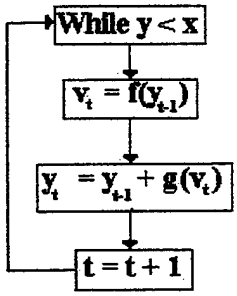

II. SIZING

There are many different ways of fitting a projectile in a rectangular barrel. At the time of this writing the design of the rail gun is still very conceptual, thus there are few physical limits placed upon the projectile.

A MATLAB computer program, provided in Appendix (A), is used to model the different possible projectile nose/body configurations as the radius of the projectile is changed. This MATLAB computer program will be referred to as the configuration comparison program. Since some of the design alternatives chosen may become invalid as the rail gun design is formalized, the equations for the configuration comparison program have been generalized. Future users of the program will be able to change inputs, such as the nose fineness ratio or the explosive payload of the projectile model, to suit new requirements and the model will still be correct.

A. CONFIGURATION ALTERNATIVES

The configuration choices made from among the different projectile design options, e.g., ogive verses spherical nose, body diameter, etc... will determine the projectile's physical dimensions. The physical dimensions, such as cross sectional area, will have a direct effect on the aerodynamic characteristics of the projectile.

1. Electrical Contact Surface

The projectile requires flat electrical contact surfaces while in the rail gun barrel. Two methods to do this are immediately evident; place the projectile in a flat-sided sabot or put flat sides on the projectile. Flat sides on the projectile for the electrical contact area are used in the model because of the two major problems with sabots outlined below.

A sabot is a spacer placed around a projectile to allow the projectile to be fired from a larger or differently shaped barrel. Sabots are usually light and often used in conventional guns when using a larger powder charge than would otherwise be possible behind a smaller projectile to increase the projectile's muzzle velocity. A sabot seems attractive from an aerodynamics consideration because the projectile can remain truly cylindrical. A cylindrical projectile should have reduced airflow separation and surface flow field turbulence. The sabot in the rail gun, however, has to conduct the electrical current required to accelerate the projectile without melting. This will require a substantial piece of metal, which equates to a large mass and thus a large inertia. This large mass will have to be accelerated with the projectile and the large inertia means it will take time to stop once it has left the barrel.

Accelerating the sabot becomes an energy consideration. The energy at the target is half the impact mass times the impact velocity squared. Since a sabot separates from the projectile immediately after leaving the barrel its mass is not present at projectile impact so the energy used to accelerate the sabot is wasted.

The large inertia associated with the sabot is a problem because the projectile will separate from the sabot as they both exit the barrel of the rail gun and the sabot will land somewhere down range. The light plastic sabots in the Phalanx gun, for example, have comparatively low velocity, high drag, and low inertia so they travel only a short distance and fall harmlessly. The sabot from the proposed rail gun's projectile will have high drag, but it will have high velocity and high inertia. This means that on long range shots the sabot may travel several miles down range and land with a high impact velocity.

Depending on the location of friendly forces and neutral populations along the line of fire, where the sabot comes down could be as important as where the projectile impacts.

Figure (3) Nose and Body Configurations

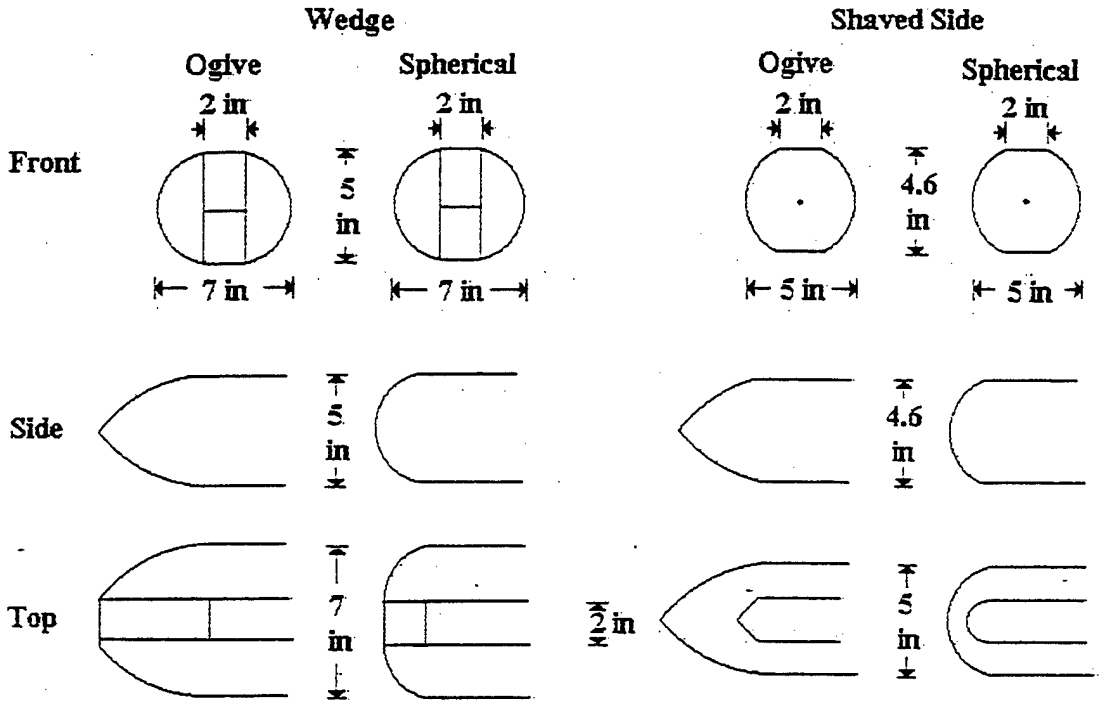

Two methods for providing flat electrical contact areas on the projectile are considered. Figure (3) above illustrates both of these methods. The first method is to slice a cylindrical projectile lengthwise down the middle and insert a rectangular wedge of appropriate width with the front of the wedge matching the curvature of the nose. The second option for providing the electrical contact surface is to shave down opposite sides of a cylindrical projectile until a sufficiently wide flat area is planed out. This reduces cross sectional area, but lengthens the projectile for the same explosive payload. Neither has an intuitive advantage over the other so both are modeled in the configuration comparison program and a choice will be made by a trade study of the output.

The width of the electrical contact area must be considered. Making the electrical contact surface smaller makes the body more cylindrical, which should reduce the separation and turbulence of the airflow around the body and therefore has aerodynamic benefit. A smaller contact area, however, means that the electric current has to go through a smaller area, which at the high currents required for rail gun operation leads to vaporization and spalling of the projectile's flat surface. Making the contact surface wider has the opposite effects of increasing separation and turbulence of airflow around the body and reducing current density. The two-inch wide contact area shown in Figure (3) is selected somewhat arbitrarily because it provides a sufficiently large electric contact area and the projectile remains fairly cylindrical. The width of the contact area is one of the physical parameters that can be changed by the user in the input section of the configuration comparison program to account for changing requirements. Since the contact surface extends the entire length of the body a narrow contact area may still provide a large electrical contact surface on both sides of the projectile. The drag equations in the configuration comparison program are written always assuming turbulent flow. Turbulent flow provides the worst drag which somewhat masks the effect of the flattened region. As specific parameters of the rail gun design are set and specific materials are chosen a smaller contact area may be possible.

2. Nose Type

There are several possible nose types for the projectile. The proposed maximum muzzle velocity of the rail gun design is Mach 8.9. The nose will experience extreme temperatures for the first several seconds after launch because of skin friction heating in the lower atmosphere and the shock front heating the air around the projectile. The high

temperatures will last until the projectile velocity is reduced, thereby reducing the strength of the shock, or the projectile reaches the upper atmosphere, where the lower air density will reduce friction.

N. Kemp and F. Riddell [Ref. 3] show the heating of a projectile's nose varies inversely with the square root of the radius of the nose's point as seen in equation (2.1).

$$Q = 20800(R_n)^{-1/2}(\rho/\rho_0)^{1/2}(u/u_c)^{3.25}(1-h_{sk}/h_{sl}) \qquad (2.1)$$

The other factors in the equation are environmental factors independent of the projectile. The temperature change of the nose is determined by equation (2.2).

$$Mc_p(dT/dt) = \Delta Q \qquad (2.2)$$

The factor ΔQ is the amount of heat being added by skin friction and the shock front minus the heat being radiated away by the nose to the atmosphere or conducted away from the nose to other parts of the projectile. A very pointed nose, meaning a small nose point radius, provides less drag, will experience more heating, and, because it has less mass over which to distribute that heat, risks melting and deforming. A very blunt nose, meaning a large nose point radius, has higher form drag, will experience less heat, and, because it has more mass over which to distribute that heat, is at reduced risk of melting and deformation. The rate at which the nose is heated and the thermal conductivity and emissivity of its constituent material determine the amount of mass required to absorb the heat without melting. If the nose is heated faster than it can radiate or diffuse the heat away if may melt or even vaporize.

A tangent ogive with a fineness ratio, nose length divided by the maximum diameter, of unity is used in the configuration comparison computer program. The fineness ratio is another of the physical parameters that the user can change in the input

section of the configuration comparison program. The user can select a fineness ratio to minimize the drag while maintaining heat capabilities for the conditions expected. A spherical nose, alternative to the tangent ogive, can also be modeled for comparison. Figure (3) on a previous page illustrates the two methods of providing the two-inch wide contact surface with both nose types and a two and one half-inch radius of body curvature.

3. Component Material

The material of which the projectile is made has important consequences on the eventual performance of the projectile. The material has to be a good conductor of both electricity and heat. A high-density material offers several advantages resulting in longer ranges and higher impact velocities.

The biggest benefit of using high density material is the increased mass per unit volume. The drag force is determined by the geometry of the projectile and the environment in which the projectile is placed. The force on the projectile equals its mass times its acceleration. If the geometry of the projectile is not changed so the drag force is constant at a point in space, but the mass is increased then the acceleration, deceleration in the case of a drag force, must decrease as shown in Figure (4) on the next page. Therefore the effect of the drag force on the velocity of the projectile is inversely proportional to the mass of the projectile. The terminal velocity of the projectile is directly proportional to the mass of the projectile as calculated by equation (2.3).

$$v_t = (2mg/\rho S_{cs} C_D)^{1/2} \qquad (2.3)$$

ρ is the ambient air density, S_{cs} is the projectiles cross sectional area, and C_D is the total drag coefficient. Another benefit of high-density material is the increased projectile penetration capabilities against hard targets.

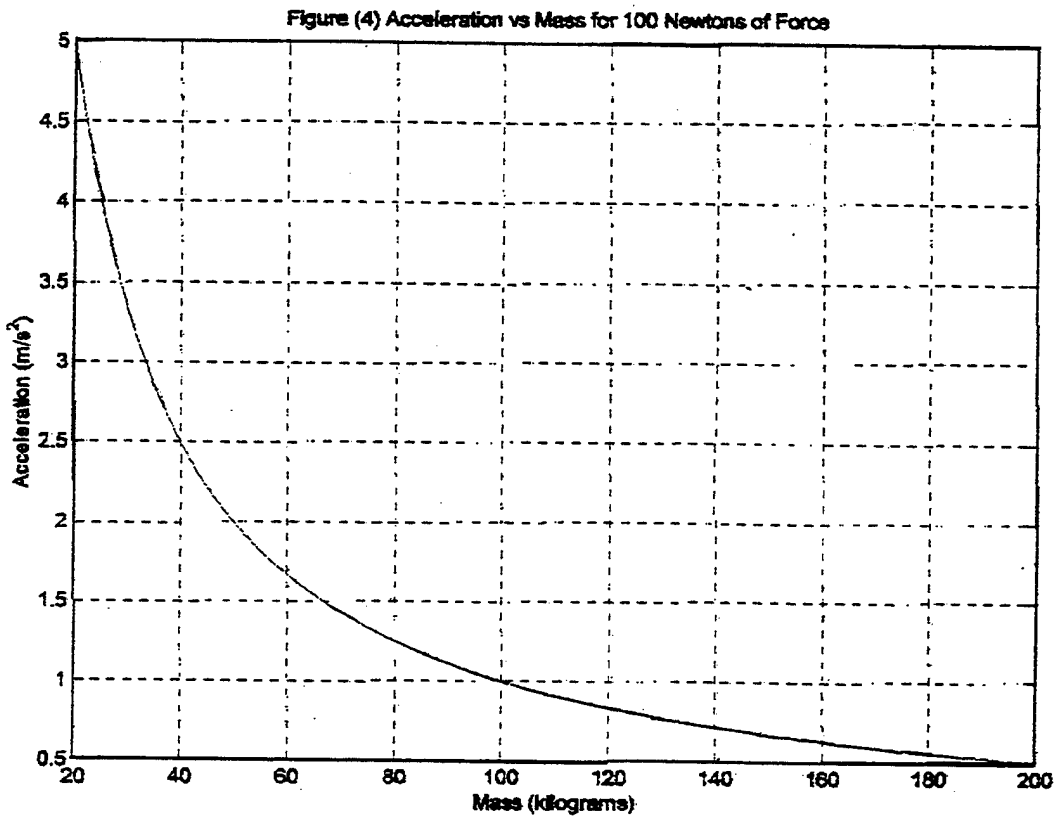

Tungsten is very dense and is already used for armor piercing projectiles. Tungsten is a good choice for this projectile and is used in the configuration comparison program for these reasons. The density of the component material can be selected by the user in the input section of the program.

As with most thing there are always disadvantages to any option. For the same reason the increased mass of a projectile made of tungsten resists the deceleration caused by drag, it also resists the acceleration by the electric and magnetic fields in the rail gun, requiring higher currents and longer barrels. Shipboard portability is another major issue

for very heavy projectiles as the individual projectiles may no longer be handled by a single sailor.

The disadvantages of large mass will probably drive an actual projectile to be made of a lighter alloy, possibly keeping an all tungsten nose for its penetration capabilities. There are limits, however, on how light a projectile can be made for a constant volume. As seen in Figure (4) the deceleration caused by drag will be greater for a lighter projectile and therefore the range and impact velocity will be little better than a conventionally fired projectile.

The configuration comparison program can use the density of any material without effecting the accuracy of the modeling. The equations in the computer program that models the trajectory of the projectile, provided in Appendix (B) and fully developed in chapter four, are written assuming that the projectile remains supersonic all the way to impact. If the projectile becomes subsonic anywhere in the trajectory the calculations in the trajectory program diverge because several of the formulas are not defined for the subsonic regime. Therefore the projectile's component material must be sufficiently dense to keep the projectile supersonic until impact.

4. Explosives

A solid metal projectile at high velocities has a great deal of kinetic energy, but at long ranges where the projectile has slowed it may need to carry explosives to be effective. Against hardened targets, such as ships or concrete structures, the sudden deceleration of the projectile at impact transfers that kinetic energy into the target. Against soft targets, such as wooden buildings or troops, there is no mechanism to rapidly convert the energy of the projectile into destructive power at the target. The destructive

power is the impact energy divided by the time over which it is transferred. The shock wave of the projectile, if it is still at a high Mach number when it reaches the target, may cause some damage because of the pressure increase with the passing of the shock wave. The higher the Mach number of the projectile the stronger the shock will be. Figure (5) on the next page, computed with an equation presented by R. Zucker [Ref. 4] used to formulate the normal shock tables, shows the upper bound, since normal shocks are the strongest shocks, of the pressure ratio as the Mach number is increased. The pressure rise caused by the shock wave quickly dissipates with distance from the projectile and the obliquity of the shock front. The projectile itself will only punch a small hole through the walls of a wooden building or into the soft dirt like a present day armor piercing shell.

Against either hard or soft targets at long ranges the projectile will decelerate to terminal velocity before impact and may not have much more kinetic energy than a convetional projectile. If the rail gun is to be a practical weapon it must be able to perform at least as well as the current weapons, such as the five inch gun it may someday replace. This means the proposed projectile will have to carry an explosive payload similar to a convetional projectile. Twelve pounds have been selected as the payload mass for the model because that is the mass of explosive material in a five inch shell. The explosive compound C4 is used in the computer model because the density of C4 is about average for modern high energy explosives. The explosive payload and the density of the selected explosive are both variables which may be changed by the user in the input section of the computer model. The length of the projectile is calculated from the volume required to contain the selected mass. Substituting a different explosive

Figure (5) Pressure Ratio for Passage of Normal Shock

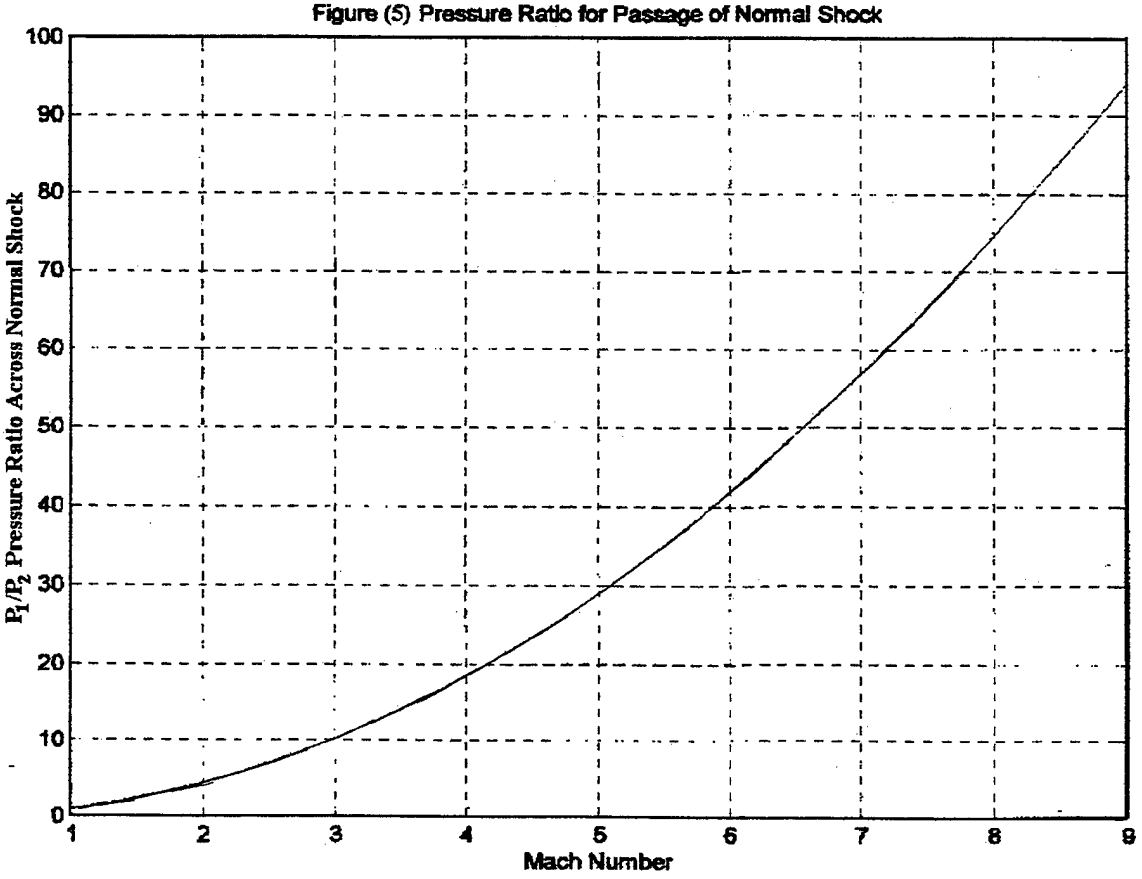

compound of similar density at the same explosive payload should only make a small difference in the length of the projectile.

5. Casing Thickness

The explosive for the projectile must obviously be encased within the projectile so the question of casing thickness arises. A casing thicker than a convetional projectile would provide more material to help absorb the expected aerodynamic heat transfer. The projectile's cross sectional area and surface area, however, will be increased for a constant explosive payload which increases the drag. The case thickness is yet another variable that a user can select in the model's input section. A half inch casing thickness was used in the model presented in the final section of this chapter.

Additional options regarding materials emerge at this point. Using a single material for the entire projectile eases manufacture since the nose and body can be cast as a single unit, so the model uses a single material, but the computer model can easily be altered to make the nose , end plate and the casing out of different materials. This is significant because the nose is not in contact with the conducting rails rails so its electric conductivity isn't very important and the casing will be the main conductor of electricity in the barrel so its conductivity is of great importance.

B. DIMENSIONS AND FORCES

This section details the development of the equations for the configuration comparison program that define the physical dimensions of the projectile's nose and body. Many of the calculations are complicated by keeping the physical dimensions as variables to allow the flexibility in the computer model discussed in the previous section.

1. Nose

The mass and surface area of the nose are the important parameters for determining the the effects of the aerodynamic properties in the equations of motion. Refering back to Figure (3) will help the reader visualize the nose configurations. To determine the mass, the volume of the nose and the mass density of its component material are required. Once the volume is determined the mass can be calculated by multiplying the volume and the density.

The geometry of the wedge insert configuration is simpler, making the required parameters easier to calculate. The volume of a half sphere and conical ogive are known formulas, the formula for the ogive can be found in Appendix A of Reference (1). The

inserted wedge for the spherical nose is just a half cylinder of the same radius and desired width. Using r as the radius of the spherical nose and h as the width of the contact area in equation (2.4).

$$NV_{s/w} = (2/3)\pi r^3 + (1/2)\pi r^2 h \qquad (2.4)$$

The calculation for the ogive wedge configuration is a little more involved. Calculus provides a convenient solution for the area of a section of a circle, shown in Figure (6) below. To get the volume we multiply the planform area that matches the nose by two and the desired width. Equation (2.5) uses L as the nose length, R as the radius of curvature of the nose, and r and h as above.

$$NV_{o/w} = \pi[L(2R^2-2Rr+r^2) - L^3/3 - (R-r)L(R^2-L^2)^{1/2} - (R-r)R^2\sin^{-1}(L/R)] + [R^2(\pi/2-\theta) - (R-r)^2\cot\theta]h \qquad (2.5)$$

Figure (6) Calculating Radius of Curvature and Planform Area for Ogive

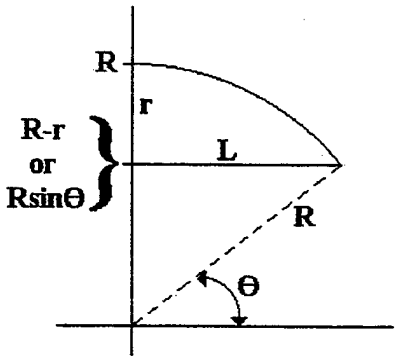

r = Radius of Projectile
L = Nose Length

Radius of Curvature of Ogive

$$R = \sqrt{L^2+(R-r)^2} \quad \text{solving for R}$$

$$R = \frac{L^2+r^2}{2r}$$

Planform Area of Ogive

$$\int_{\theta}^{\frac{\pi}{2}} \int_{(R-r)\csc\theta}^{R} r\,dr\,d\theta \quad \text{where } \theta = \cos^{-1}\frac{L}{R}$$

solving the integrals

$$\frac{1}{2}[R^2(\frac{\pi}{2}-\theta)-(R-r)^2\cot\theta]$$

The volume of the shaved side projectile configuration is easily understood in concept, but mathematicaly complicated to compute. The concept is simply to determine the volume for the complete nose shape and subtract the volume of the piece that is

shaved away. The removed volume is determined by solving the triple integral in equation (2.6).

$$RV = \int_0^{h/2} \int_{\cos^{-1}(fz/R)}^{\pi/2} \int_{(R^2 - f^2z^2)^{1/2}\csc\theta'}^{R} r'\, dr'\, d\theta'\, dz \qquad (2.6)$$

The term f is the nose fineness ratio. Completing the integration with variables for the limits of integration requires an approximation. Simpson's Rule is used to get the solution of the integral above for equation (2.7):

$$\begin{aligned} RV = {} & R^2h\pi/8 - (R^2h/4)\cos^{-1}(fh/2R) - (R^3/2f)(1-(fh/2R)^2)^{1/2} + R^3/2f - \\ & (Rfh/48)[(h/2)\csc(\cos^{-1}(hf/8R)) + (h/2)\csc(\cos^{-1}(hf/4R)) + \\ & \quad (3h/2)\csc(\cos^{-1}(3hf/8R)) + (h/2)\csc(\cos^{-1}(hf/2R))] + \\ & (f^3h/48R)[(h^2/128)\csc(\cos^{-1}(hf/8R)) + (h^2/32)\csc(\cos^{-1}(hf/4R)) + \\ & \quad (27h^2/128)\csc(\cos^{-1}(3hf/8R)) + (h^2/8)\csc(\cos^{-1}(hf/2R)) \end{aligned} \qquad (2.7)$$

Multiplying this volume by four gives the total volume lost from the nose by planing the flat sides on to the projectile. A spherical nose is the limiting case of the ogive nose where the fineness ratio equals one half, the radius of curvature of the nose and the length of the nose equal the radius of the projectile. The volume equation for the shaved side spherical nose configuration is equation (2.8).

$$\begin{aligned} NV_{s/s} = {} & (2/3)\pi r^3 - R^2h\pi/2 + R^2h\cos^{-1}(h/4R) + 4R^3(1-(h/4R)^2)^{1/2} - R^3 + \\ & (Rh/24)[(h/2)\csc(\cos^{-1}(h/16R)) + (h/2)\csc(\cos^{-1}(h/8R)) + \\ & \quad (3h/2)\csc(\cos^{-1}(3h/16R)) + (h/2)\csc(\cos^{-1}(h/4R))] - \\ & (h/96R)[(h^2/128)\csc(\cos^{-1}(h/16R)) + (h^2/32)\csc(\cos^{-1}(h/8R)) + \\ & \quad (27h^2/128)\csc(\cos^{-1}(3h/16R)) + (h^2/8)\csc(\cos^{-1}(h/4R)) \end{aligned} \qquad (2.8)$$

The volume for the shaved side ogive nose configuration is shown in equation (2.9):

$$\begin{aligned} NV_{o/s} = {} & \pi[L(2R^2-2Rr+r^2) - L^3/3 - (R-r)L(R^2-L^2)^{1/2} - (R-r)\sin^{-1}(L/R)] - \\ & R^2h\pi/2 + R^2h\cos^{-1}(fh/2R) + (2R^3/f)(1-(fh/2R)^2)^{1/2} - 2R^3/f + \\ & (Rfh/12)[(h/2)\csc(\cos^{-1}(hf/8R)) + (h/2)\csc(\cos^{-1}(hf/4R)) + \\ & \quad (3h/2)\csc(\cos^{-1}(3hf/8R)) + (h/2)\csc(\cos^{-1}(hf/2R))] - \\ & (f^3h/12R)[(h^2/128)\csc(\cos^{-1}(hf/8R)) + (h^2/32)\csc(\cos^{-1}(hf/4R)) + \\ & \quad (27h^2/128)\csc(\cos^{-1}(3hf/8R)) + (h^2/8)\csc(\cos^{-1}(hf/2R)) \end{aligned} \qquad (2.9)$$

The surface area of the various nose configurations, needed to determine skin friction drag. Once again the wedge insert configuration surface areas were easier to calculate. The spherical nose with wedge insert is the surface area of a half sphere plus the surface area of half a cylinder of matching radius and desired electrical contact area width. The formula for the spherical nose with wedge insert is given in equation (2.10):

$$S_{ns/w} = 2\pi r^2 + \pi rh \tag{2.10}$$

The equation for the surface area of the ogive nose is a surface of revolution and is determined by solving the integral in equation (2.11):

$$S_o = \int_0^{2fr} 2\pi[(R^2-y^2)^{1/2} - (R-r)][1+(y^2/(R^2-y^2)]^{1/2}\ dy = 2\pi[2frR - R(R-r)\sin^{-1}(2fr/R)] \tag{2.11}$$

The surface area of the inserted wedge is the desired electrical contact area width and the arc length, which is determined from the radius of curvature of the nose and θ as calculated in Figure (6), doubled to account for the upper and lower surface of the wedge. The surface area of the ogive nose with wedge insert is the surface area of the ogive nose plus the surface area of the wedge insert, shown in equation (2.12).

$$S_{no/w} = 2\pi[2frR - R(R-r)\sin^{-1}(2fr/R)] + 2hR\theta \tag{2.12}$$

The surface area of the shaved side configuration is calculated in much the same manner as the volume was determined. The surface area of the removed section is subtracted form the surface area of the whole surface, but now the surface area of the remaining flat surface must be added back to the surface area. For the shaved side spherical nose one can use the symmetry as we did in the volume calculation. The removed surface area can be considered a surface of revolution and determined by solving the integral in equation (2.13).

$$\int_0^{.5h} 2\pi y(1+(dy/dx)^2)^{1/2}\,dx = 2\pi[\{-.5r\ \ln(.5h + (r+.25h^2)^{1/2})\} + \{.25h(r+.25h^2)^{1/2}\} + \{.5r\ \ln(r)\}] \quad (2.13)$$

The integrand in equation (2.13) is $y = (r^2-x^2)^{1/2}$ and the limits of integration are from the centerline of the projectile to the edge of the flat electrical contact surface. Each of the resulting flat areas left on the nose is a half circle with a radius of one half the electrical contact area width. Collecting all the terms for the surface of the half sphere, the surface of the removed portion, and the surface of the remaining flat spots results in equation (2.14).

$$S_{ns/s} = 2\pi r^2 - 2\pi[\{-.5r\ \ln(.5h+(r+.25h^2)^{1/2})\} + .25h(r+.25h^2)^{1/2}\} + \{.5r\ \ln(r)\}]+ \pi(h/2)^2 \quad (2.14)$$

The shaved side ogive nose is harder to calculate because of the lack of symmetry. The removed surface area for the shaved side ogive nose is four times the value of the double integral solved in equation (2.15).

$$\int_0^{h/2}\int_0^{(\pi/2 - \cos^{-1}(fz/r))} R\,d\theta\,dz = R[\pi h/4 - (h/2)\cos^{-1}(fh/2R) - (R/f)(1-(fh/2R)^2)^{1/2} + R/f] \quad (2.15)$$

The flat area left on the nose when the sides are shaved down is once again shaped like the area in Figure (6). The surface area of the ogive nose with shaved sides configuration is the combination of the surface area of the ogive nose minus the surface area of the removed section plus the surface area of the flat spots left on the nose when the shaved area is remove. The ogive nose with shaved sides surface area formula is given by equation (2.16).

$$S_{no/s} = 2\pi[2frR - R(R-r)\sin^{-1}(2fr/R)] - R[\pi h - (2h)\cos^{-1}(fh/2R) - (4R/f)(1-(fh/2R)^2)^{1/2} + 4R/f] + 2[R^2(\pi/2-\cos^{-1}(h/R)) - (R-h/2)^2\cot(\cos^{-1}(h/R))] \quad (2.16)$$

2. **Body**

The cross sectional area, length, mass, and surface area are the important physical characteristics of the projectile body. The cross sectional area of the wedge insert configuration is the area of a circle who's radius is the radius of the projectile plus the area of a rectangle who's height is twice the radius and who's width is the width of the contact area, as shown in equation (2.17).

$$S_{csw} = \pi r^2 + 2rh \quad (2.17)$$

The cross sectional area of the shaved side configuration is the area of a circle minus four of the planform areas that were calculated for the shaved side spherical nose, shown in equation (2.18).

$$S_{css} = \pi r^2 - 2[r^2(\pi/2-\theta) - (r-r')^2\cot\theta] \quad (2.18)$$

The length of the projectile's body depends on how much explosive is required. First the cross sectional area of the explosive must be determined for the desired projectile radius and skin thickness. The same equations as were used for the body's cross sectional area can be used to determine the explosive's cross sectional area by reducing the radius used in the equation by the desired skin thickness. The length can now be determined by dividing the desired explosive payload mass by explosive cross sectional area and the density of the chosen explosive. Equation (2.19) uses m_e as the mass of the explosive, ρ_e as the density of the explosive, and S_{ecs} as the appropriate explosive cross sectional area for the wedge or shaved configuration.

$$L_b = m_e/\rho_e S_{ecs} \quad (2.19)$$

The mass of the projectiles body is the sum of the explosive mass plus the mass of the casing material. To determine the mass of the casing it is easiest to find the volume of the material by subtracting the explosive cross sectional area from the projectile's cross sectional area and multiplying by the length of the explosive and density of casing material. Equation (2.20) uses the variables from above and S_{pcs} for projectile cross sectional area, ρ_c for the density of the casing material, L_b for the body length, and m_b for mass of the body.

$$m_b = m_e + L_b\rho_c(S_{pcs} - S_{ecs}) \tag{2.20}$$

Of course the length and cross sectional areas must all be for the same wedge or shaved configuration.

The body's surface area for the wedge insert configuration is, again, easily determined. It is the surface area of a cylinder plus the upper and lower contact surface which is the width of the contact area times the length of the body as shown in equation (2.21).

$$S_{bw} = 2\pi rL_{bw} + 2hL_{bw} \tag{2.21}$$

The shaved side configuration requires reference back to Figure (3). In order to get the arc length to determine the surface area the figure should be viewed on its' side. For this case we know that $R\sin\theta$ equals half the contact area width where R is the radius of the projectile. Solving for θ and multiplying by the radius determines half the arc length for one side of the projectile. Multiplying the arc length by four and by length of the shaved side body gives the surface area of the curved portions of the projectile body. The flat surfaces on the projectile are once again the contact area width times the body length for the shaved side configuration. Combining the surface areas for the shaved side

configuration we get equation (2.22), the total surface area for the body in this configuration:

$$S_{bs} = 4rL_{bs}\sin^{-1}(h/r) + 2hL_{bs} \tag{2.22}$$

3. **End Plate**

The end plate is assumed to be the same thickness as the casing, although this can be changed in the programs if desired. Since the thickness is set the only parameters to find are the surface area and mass. The surface area can be easily calculated by taking the equation for the body surface area for the matching configuration from the previous section and replacing the body length with the skin thickness. The mass is just as easily determined by multiplying the cross sectional area of the matching body configuration by the skin thickness and component material density.

4. **Drag**

The form and skin friction drag for the different projectile configurations are computed using Reference (1) to compare the drag characteristics of each. The dynamic head is required for drag calculations and is computed in the model using standard sea level air density and the selected muzzle velocity with equation (2.23):

$$q = (1/2)\rho v^2 \tag{2.23}$$

The skin friction drag is computed using a generic high velocity skin friction drag coefficient form Reference (1) of .002. The generic skin friction drag coefficient is an acceptable approximation because the large velocity of the projectile is the same for all cases and dominates the numerator of the Reynolds number calculation, shown in equation (2.24) used to determine an exact skin friction drag coefficient, shown in equation (2.25).

$$Re = \rho v L_T/\mu \tag{2.24}$$

$$C_f = .455\ [Log_{10}(Re)]^{-2.58} \tag{2.25}$$

The skin friction drag, equation (2.26), is the skin friction drag coefficient multiplied by the total surface area and the dynamic head.

$$C_{Df} = C_f S q \tag{2.26}$$

The form drag calculation has a few more intermediate steps. The form drag coefficient multiplied by the projectile's cross sectional area, S_{pcs}, and the dynamic head previously calculated determines the form drag in equation (2.27):

$$C_{DF} = C_F(S_{pcs})q \tag{2.27}$$

The form drag coefficient is calculated with equation (2.28):

$$C_F = (\Delta p/q)\{1-[(196(L_n/d)^2-16)/(14(M+18)(L_n/d)^2)]\} \tag{2.28}$$

The conical shock pressure coefficient is calculated using the empirical formula given in equation (2.29).

$$\Delta p/q = [.083+(.096/M^2)](\sigma/10)^{1.69} \tag{2.29}$$

The semivertex angle, σ, of a reference cone corresponding to the ogive nose is required to determine the pressure rise across a conical shock and is determined in equation (2.30) by taking the arctangent of one divided by twice the fineness ratio.

$$\sigma = \tan^{-1}(1/2f) \tag{2.30}$$

B. RESULTS

The configuration comparison computer program computes the physical data for the projectile over a range of projectile radii selected by the user for the different projectile configurations and plots the results for comparison. Figures (7) through (12) on the next several pages presents these plots for one computer program run with the

Figure (7) Form Drag vs Skin Friction Drag at Sea Level, V0=3000 km/s

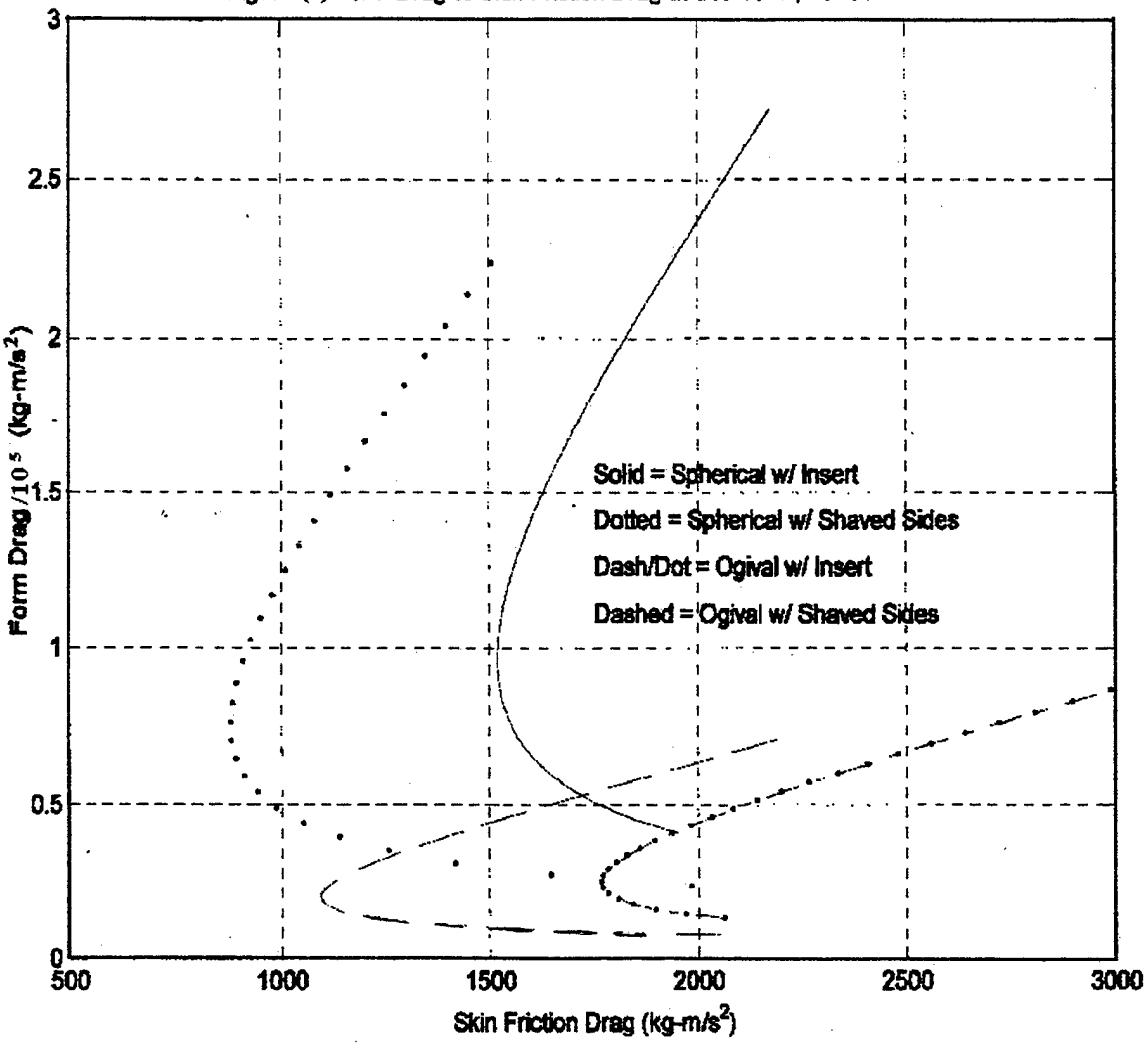

Figure (8) Form Drag vs Width at Sea Level, V0=3000 km/s

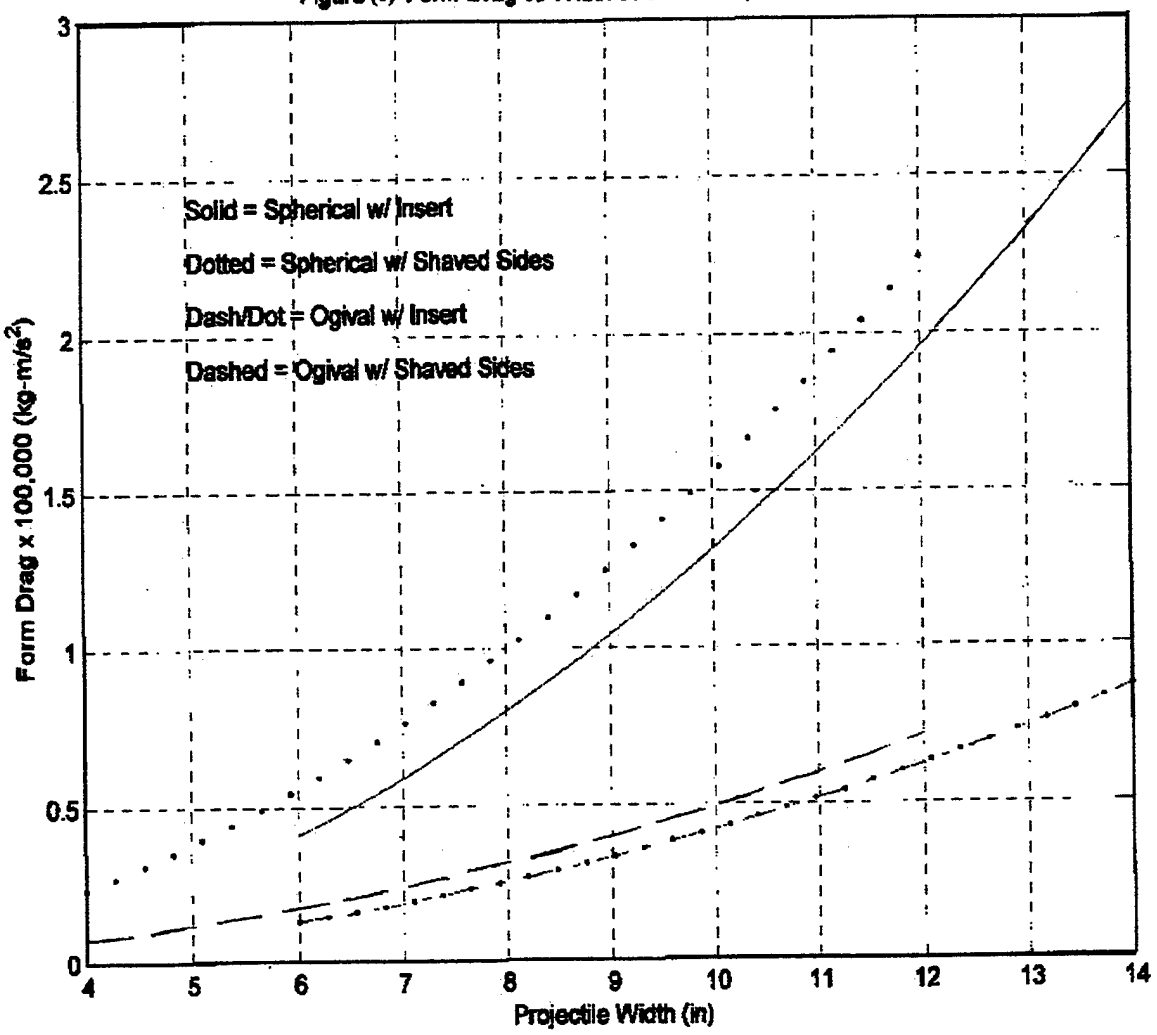

Figure (9) Length vs Width

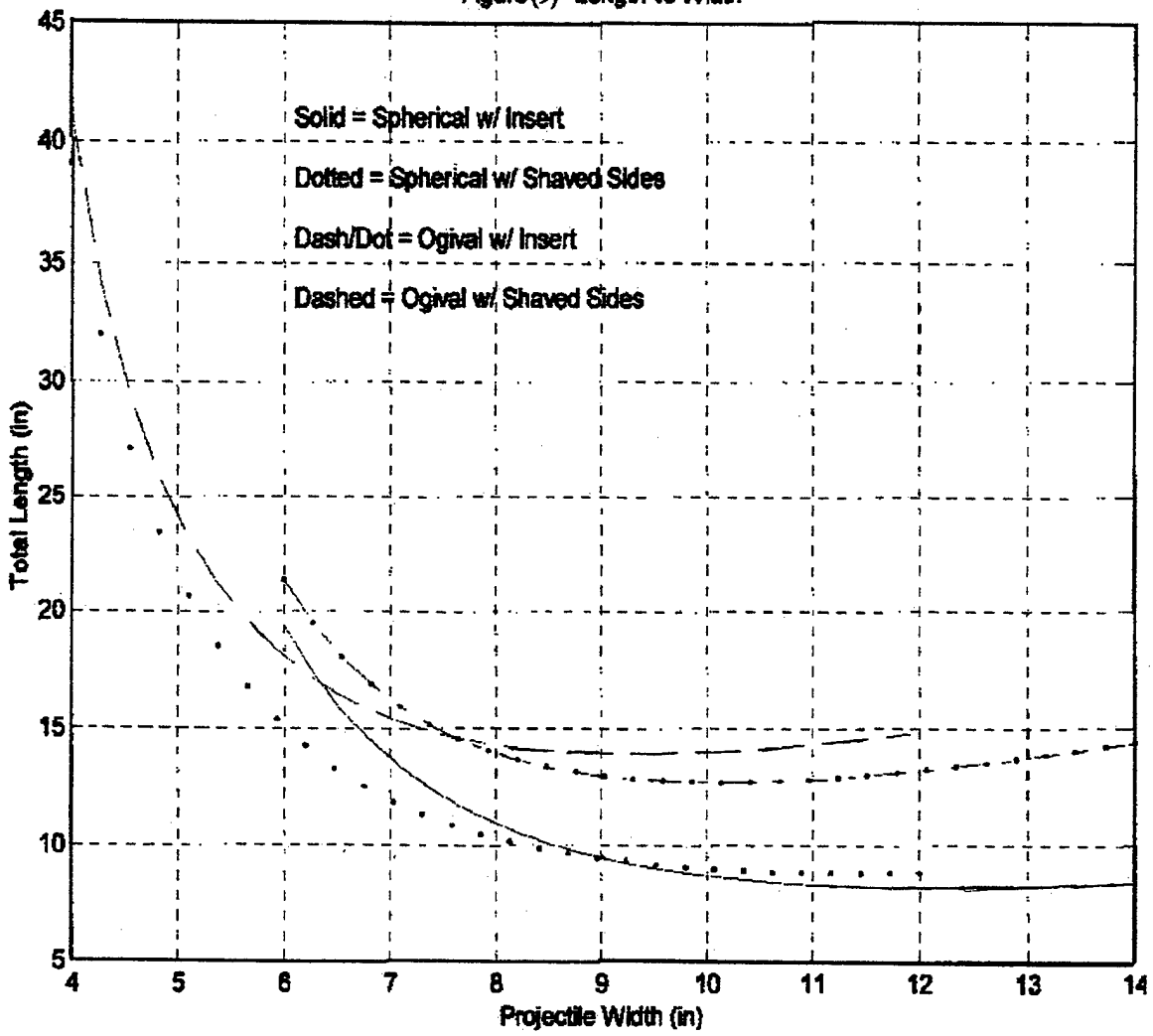

Figure(10) Weight vs Width

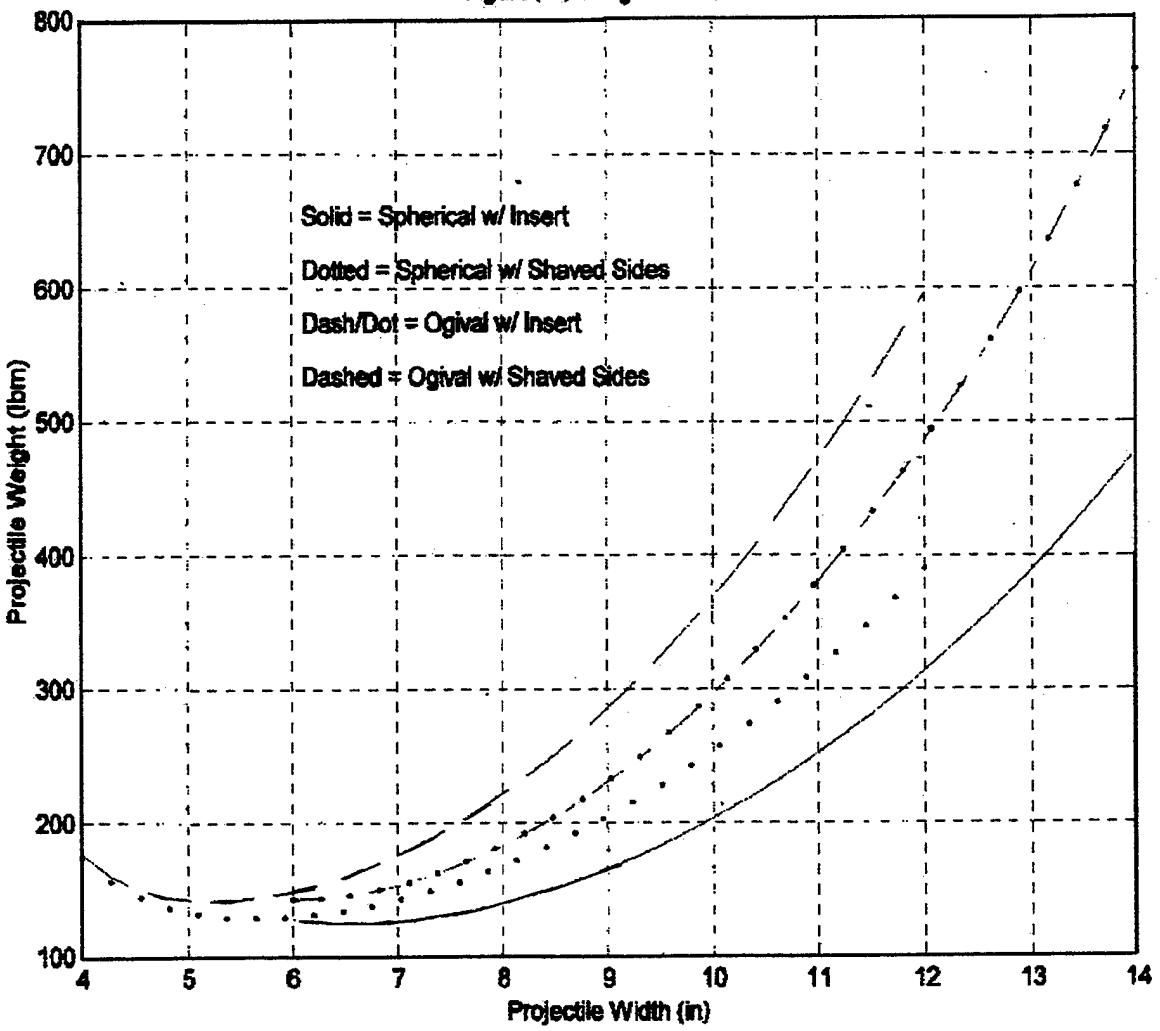

Figure (11) Length vs Weight

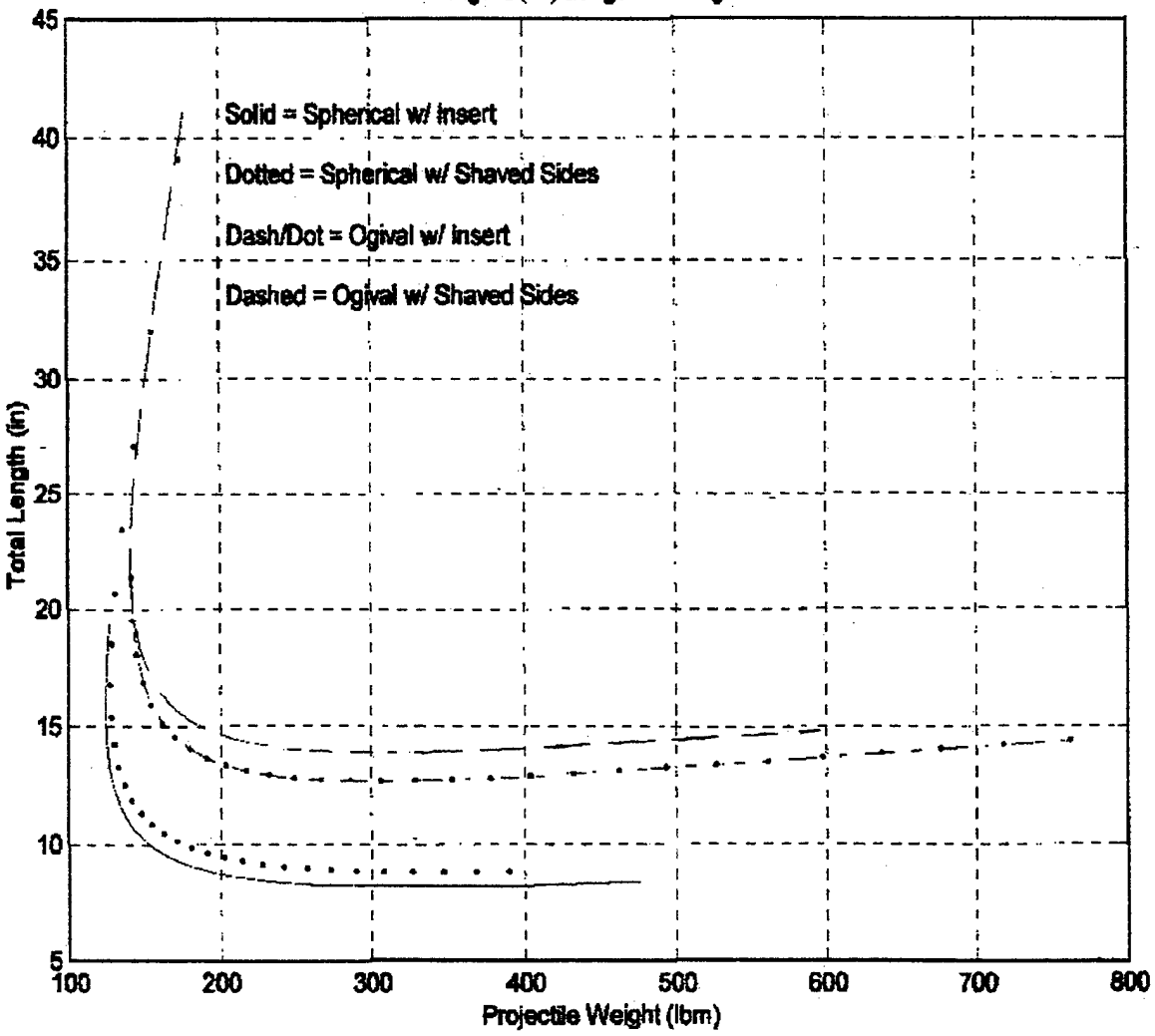

Figure (12) Skin Friction Drag vs Width at Sea Level, V0=3000 km/s

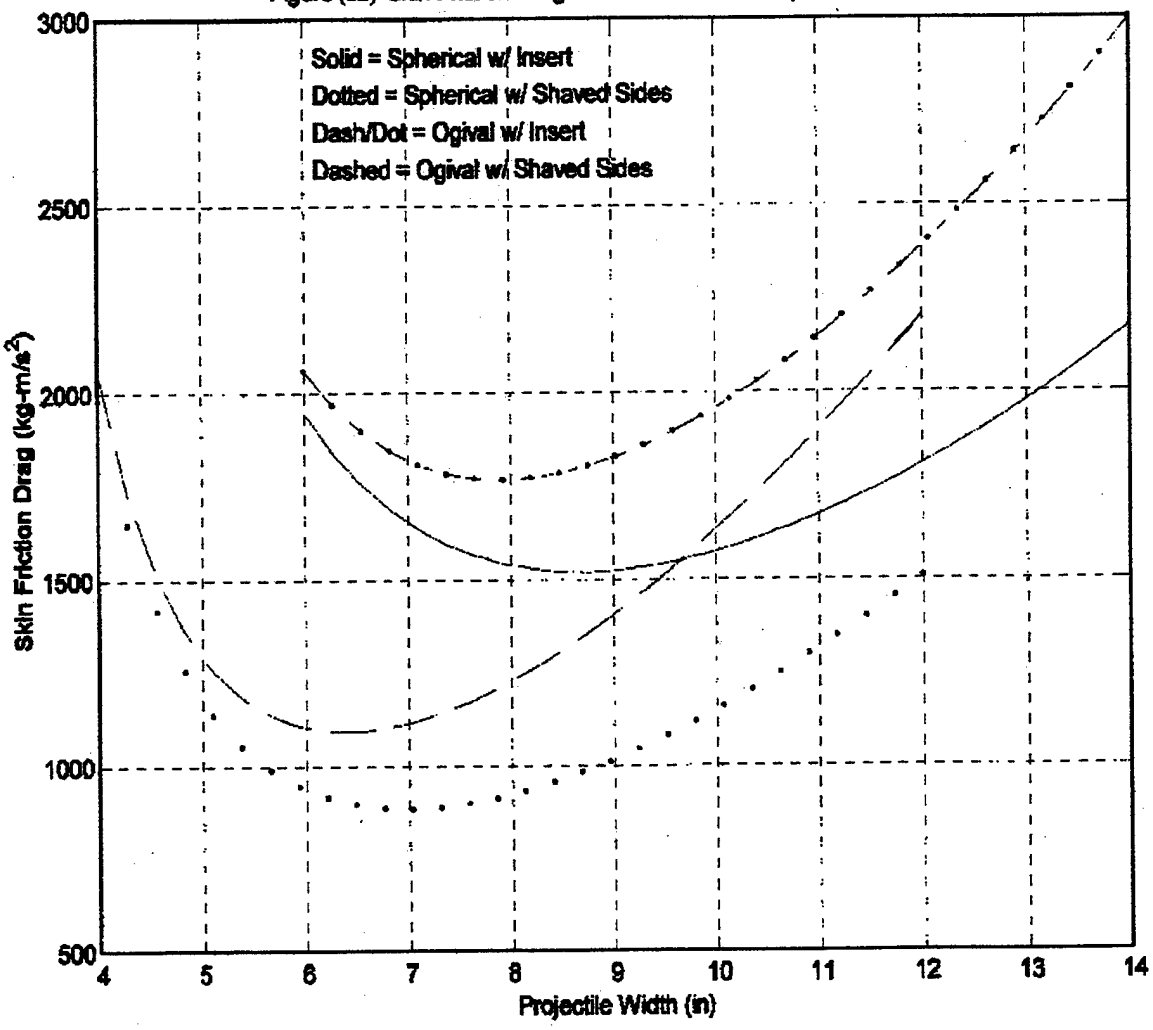

projectile radius ranging from two to six inches. The majority of the inputs and the plots are in English units, but the model can display the plots in SI units by minor modifications to the variables in the plot statements.

If the only consideration is to maximize the range and impact energy of the projectile, then minimizing the total drag will optimize the projectile's performance. The form drag is two orders of magnitude larger than the skin friction drag in Figure (7) so the minimum total drag is along the bottom of the plot.

Examining Figure (8) shows that the minimum form drag is the shaved side ogive configuration with a four-inch diameter. Refering to Figure (9) the four inch wide shaved side ogive projectile is forty one inches long. That is not a very practical length. Figure (10) or Figure (11) shows that the projectile would weigh one hundred and seventy-eight pounds.

The five inch diameter shaved side ogive projectile has only slightly higher form drag as shown in Figure (8) and substantially lower skin friction drag shown in Figure (12). The length of the five inch shaved side ogive projectile in Figure (11) is twenty four inches. Twenty four inches is a far more practical length for many reasons. A twenty four inch projectile is easier to store, will have less longitudinal stresses in flight, and the explosive material is easier to detonate when it is packed together rather than stretched out. Refering to Figure (10) or Figure (11) the five inch shaved side projectile would weigh one hundred and forty-four pounds.

Using the same figures as the previous two cases, the six inch diameter shaved side ogive projectile is shorter still at only fifteen inches in length, but the form drag is beginning to get appreciably larger. The skin friction drag for the six inch shave side

ogive projectile is actually the minimum, but the form drag increase is substantially larger than the skin friction drag decrease. The six inch shaved wide projectile would weigh one hundred and forty-seven pounds. The increased drag without increased weight would mean a decrease in performance.

Many of the assumptions made in defining the inputs to run the model were selected with the idea of replacing a conventional five inch gun with a rail gun, so it should be no surprise that a modified five inch projectile is the apparent best choice. As other requirements are specified the plots can be used to make similar comparisons between the parameters to best meet the desired performance. There are additional plots produced by the configuration comparison program that weren't needed for the above analysis, but may be useful for other comparisons. Many more parameters are calculated in the model than are plotted. A user can change or add plot commands to get the plots necessary to make the comparisons they desire for the requirements they are given.

III. STABILITY

Projectiles fired over any appreciable distance require some form of stability to keep from being tumbled by minor variations in wind speed i.e., wind shear. Projectiles fired from conventional guns are spun in the barrel so they have angular momentum to provide stability. The proposed rail gun barrel, being rectangular, will not impart this angular momentum to its projectile. Fins are the most practical means of providing a stabilizing force.

A stability program, also written in MATLAB and provided in Appendix (C), models the stability of a projectile with fins. The shaved side projectile configuration appears better able to provide long range and high impact velocity than the wedge insert configuration because of the shaved side's lower drag. Therefore, the shaved side configuration is modeled in the stability program. The equations for the ogive nose are used in the model, but if a spherical nose is desired it is simply an ogive with a fineness ratio of one half.

A. FINS

A variety of ideas were initially considered for attaching the stabilizing fins to the projectile. Most of the ideas considered for attaching fins were concerned with whether or not there was sufficient room in the barrel to accommodate fins large enough to provide stability. Attaching large fins requires that they be at least partially retracted while in the barrel of the rail gun and that they deploy after the projectile has left the barrel. Folding fins add complexity and, as such, cost to the over all system.

Selecting short span fins with long chord, as shown in Figure (13) on the next page, it will be shown will provide the stability without adding the complexity and cost of

Figure (13) Short Span Long Chord Fin

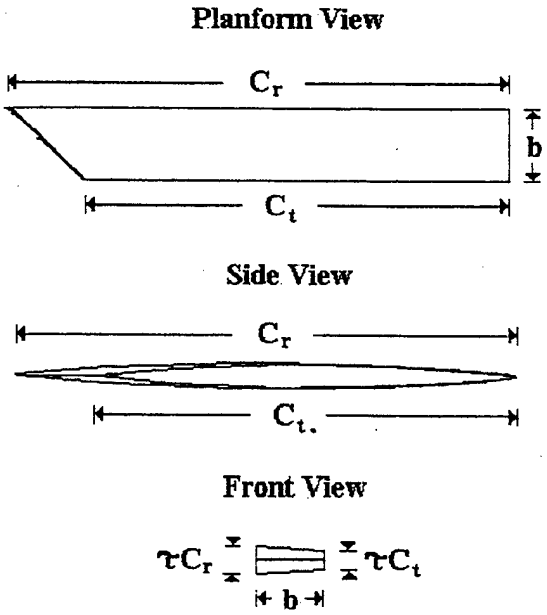

a folding fin configuration. A cruciform configuration with the fins extending to the corners of the rectangular barrel is probably the simplest configuration and is what was shown in Figure (1). Symmetric biconvex fins are used in the stability program because, as per Reference (1), they are easy to manufacture and offer the best structural strength.

The dimensions for the nose and body are calculated with the shaved side ogive nose equations developed in the previous chapter. The dimensions of the fins are calculated by the model using several inputs from the user and values from the nose and body calculations.

1. Span and Chord

The span of the individual fins is calculated in equation (3.1) by subtracting the radius of the projectile from the hypotenuse of a triangle whose sides are half the projectile diameter at the shaved surfaces.

$$b = [(r-r')^2+(r-r')^2]^{1/2} - r \qquad (3.1)$$

Calculating the span in this way keeps the fins orthogonal to each other and keeps their length correct to just touch the barrel wall regardless of selected projectile radius. Many of the aerodynamic calculations assume the fins in pairs without the body present to form a clipped delta whose span is just twice the individual fin's span.

The root chord is determined as a user selected percentage of the total body length calculated for the selected body radius. The tip chord is calculated in equation (3.2) by multiplying the span by the tangent of the sweep angle of the fin's leading edge, Λ, and subtracting the result from the root chord of the fin.

$$C_t = C_r - b\tan\Lambda \tag{3.2}$$

The selected chord length has two effects in the calculations of the other physical dimension. The longer the chord length, the shorter the span can be while still providing stabilization of the projectile. The thickness of the fin is determined by multiplying the chord by a user inputted thickness to chord ratio, τ. The longer the chord length, the thicker the fin becomes which increases form drag. Users are cautioned to remain conscious of the thickness of the fins as form drag caused by unnecessarily thick fins may severely degrade the performance of the projectile.

The sweep angle is set in the stability program to keep the leading edge of the fin forward of the Mach cones created at the point of the delta, which keeps the leading edge supersonic until the freestream becomes transsonic. If a user is sure that the projectile will never slow to transsonic velocities, a larger sweep angle may be used without the calculations, such as for the fin form drag coefficient, diverging. The sweep angle is set in the fins section of the program rather than in the input section to prevent inexperienced users from getting in trouble by making a poor selection of sweep angle.

2. Surface Areas

The planform area of a fin pair is used as a reference area in many intermediate calculations relating to the fins, all the final quantities are referenced to the maximum body cross sectional area. The simplest way to calculate the planform area is to break up the fin pair into a pair of triangles and a rectangle. The area of the two triangles is the the root chord minus the tip chord multiplied by the span. The rectangle is the tip chord multiplied by the span of a fin pair. Equation (3.3) combines the terms.

$$S_f = (C_r - C_t)b + 2C_t b \tag{3.3}$$

Since the fin configuration is a clipped delta wing some of the calculations are based on what percentage of the full delta wing is present, so the planform of the full delta wing is required. The planform of the full delta wing is the root chord multiplied by half the span, as shown in equation (3.4)

$$S_d = C_r b \tag{3.4}$$

3. Volume and Mass

The thickness of the fin is determined from a thickness to chord ratio, τ, so as the chord lessens from root to tip so does the fin thickness. This makes determining the volume of the fins very difficult. Since the fins do not have a large sweep angle and do have a very short span using the surface area of a rectangular fin with the mean aerodynamic chord of the actual fin offers a very close approximation to the surface area of the actual fin. The mean aerodynamic chord for a clipped delta wing is calculated with equation (3.5):

$$C_{ma} = (2/3)C_r\{[1+(C_t/C_r)+(C_t/C_r)^2]/[1+(C_t/C_r)]\} \tag{3.5}$$

The volume can now be approximated by determining a rectangular fin cross sectional area at the mean aerodynamic chord and multiplying it by the span. To determine the fins cross sectional area the equations from Figure (6) can be used once again. The symmetry of a rectangular biconvex wing allows the calculation for a single section to be multiplied by four to get the total volume. The volume of the fins and the intermediate steps required to calculate it are shown in equations (3.6), (3.7), and (3.8).

$$R_f = [(.5C_{ma})^2 + (.5\tau C_{ma})^2]/\tau\, C_{ma} \tag{3.6}$$

$$\theta_f = \cos^{-1}(.5C_{ma}/\, R_f) \tag{3.7}$$

$$V_f = 4b[(R_f)^2(\pi/2 - \theta_f) - (R_f - .5\tau C_{ma})\cot\theta_f] \tag{3.8}$$

The mass of the fins can then be calculated in equation (3.9) by multiplying the volume by two, for the two fin pairs, and the density of the component material.

$$m_f = 2\, V_f \rho_c \tag{3.9}$$

B. MATHEMATICAL MODEL

The physical dimensions calculated are now use to determine aerodynamic coefficients. The combination of the aerodynamic coefficients will be used to determine if the projectile is stable.

1. Center of Gravity

The center of gravity is required to calculate the stability. Since the projectile is symmetric along its length the simplest method of calculating the center of gravity is to add the first moments of all the components, which will all be on the center axis, and divide by the total mass. Placing the origin at the point of the nose the first moment equations for the nose, body, end plate, and fins become equations (3.10), (3.11), (3.12), and (3.13) respectively.

$$I_n = .707(2fr)m_n \quad (3.10)$$

$$I_b = [.5L_b+2fr][\rho_c L_b(S_{pcs}-S_{ecs})+m_e] \quad (3.11)$$

$$I_{ep} = [.5(st)+L_b+2fr][\rho_c(st)(S_{pcs})] \quad (3.12)$$

$$I_f = [.5C_{ma}+(1-(\%+.1))L_T][2m_f] \quad (3.13)$$

The percent sign is the root chord percentage of body length and L_T is the total projectile length.

2. Graphical Approximations and Miscellaneous Factors

Many aerodynamic coefficients and factors are determined empirically and given in graphical form. The four interference factors from Reference (2) and the nose/body lift coefficient from Reference (5) are presented graphically and are required for several of the calculations. The user of the stability program would have to calculate many of the projectile's physical parameters to read the graphs and find the correct inputs to the program everytime a parameter, such as projectile radius or root chord percentage, was changed. Having the user do many of the calculations defeats the purpose of having a computer model. Computers, unfortunately, cannot read graphs so it became necessary to determine equations that the computer could use to calculate the values of coefficients and factors. Appendix (D) has a series of short MATLAB programs written to determine curves that match the graphs from the above references. The plots from these MATLAB programs are provided in Appendix (D) with several points, corresponding to actual points from the references, marked for accuracy comparison. Reviewing these plots will reveal that the approximations are seldom more than a couple of percent off.

There are several calculated aerodynamic quantities that are used in the equations. The aspect ratio calculated in equation (3.14) is the square of the span divided by the planform area of the fin.

$$AR = b^2/S_f \tag{3.14}$$

The Mach angle μ is the angle of the semivertex of the Mach cone and is determined in equation (3.15) by taking the inverse sine of the inverse of the Mach number.

$$\mu = \sin^{-1}(1/M) \tag{3.15}$$

The final quantity is β, which is the square root of the Mach number squared minus one, shown in equation (3.16).

$$\beta = (M^2 - 1)^{1/2} \tag{3.16}$$

3. Center of Pressure

The center of pressure of the nose/body is also a graph determined quantity from Reference (5), but the plot is a fixed straight line so long as the body length is at least twice the nose length. Similar to the nose/body lift coefficient, shown in Appendix (4), the center of pressure graph is divided into two separate lines at the point where β divided by the nose fineness ratio equals one. An if/then statement in the stability program determines when β divided by the nose fineness ratio is less than or equal to one and then calculates the two quantities with equations (3.17) and (3.18):

$$CN_{\alpha n} = -.28[(\beta/f)-1.9]^2 + 3.58 \tag{3.17}$$

$$X_{CPn} = CG - [(.125L_T\beta/f)+.15] \tag{3.18}$$

The center of pressure is referenced to the center of gravity. If β divided by the nose fineness ratio is greater than one the program uses equations (3.19) and (3.20):

$$CN_{\alpha n} = -3.4[(f/\beta)-.9]^2 + 3.4 \tag{3.19}$$

Figure(14) Mach Cones on Fin Planform

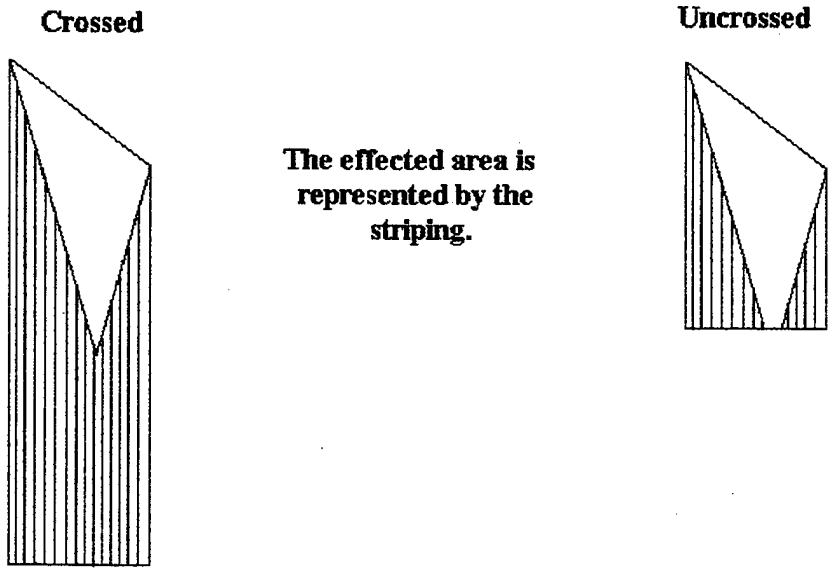

$$X_{CPn} = CG - [(-.125L_T f/\beta)+.425] \qquad (3.20)$$

The area of the fin effected by the Mach cones created at the point of the delta and at the fin tips is defined by the μ calculated above. The effected surface area will increase as the Mach number decreases and decrease as the Mach number increases. The effected area has a lift coefficient that is half the coefficient for the fin surface in the uneffected area and is thus an important intermediate step in calculating the total lift coefficient and center of pressure location of the fins. Calculating the effected surface area is also done by dividing the calculation into two regions. If the span is short and the root chord is long, as in Figure (1), the Mach cones will cross somewhere on the fin's surface, but if the root chord gets shorter and the span longer or the Mach number gets very large the Mach cones may not cross until after the fin's trailing edge, as shown in Figure (14) above. In order not to double count the effected surface area another if/then statement is used. Whether the Mach cones have crossed before the trailing edge is

determined by adding the base at the fin's trailing edge of the triangles formed on the planform surface by the Mach cones and comparing to see if that exceeds the span. If the Mach cones have crossed the unaffected planform area is computed and subtracted from the total fin planform area with equation (3.21).

$$S_{eff} = S_f - \{[(1.1452\tan(\pi/2-\Lambda-\mu))/(\tan(\pi/2-\Lambda-\mu)+\tan(\Lambda-\pi/2-\mu))]^2 + [(1.1452\tan(\Lambda-\pi/2-\mu))/(\tan(\pi/2-\Lambda-\mu)+\tan(\Lambda-\pi/2-\mu))]^2 \}\tan(\pi/2-\Lambda-\mu) \quad (3.21)$$

If the Mach cones do not cross the calculation of the effected planform surface area is simply the addition of the surface area of the two triangles formed by the Mach cones shown in equation (3.22).

$$S_{eff} = C_r^2 \tan\mu + C_t^2 \tan\mu \quad (3.22)$$

The normal force coefficient of the fins can now be determined. If there were no Mach cones the normal force coefficient would simply be four divided by the quantity β. The effected area in the Mach cones, however, only has a normal force coefficient that is half the value for the uneffected area, two divided by the quantity β. To account for the reduced lift coefficient in the effected area half the lift coefficient multiplied by the percentage of total fin planform area effected is subtracted from the total as shown in equation (2.23).

$$CN_{\alpha f} = (4/\beta) - (2S_{eff}/\beta S_f) \quad (2.23)$$

The center of pressure for a full delta wing is simply two thirds the root chord. Since the fins being used are basically clipped delta wings the center of pressure is moved forward and related to what percentage of the full delta wings area is actually present. The center of pressure of the fin is also effected by the Mach cones. The Mach

cone effected area only counts as half its actual area as a percentage of the total delta wing area. The center of pressure for the fin is calculated by equation (3.24).

$$X_{CPf} = (2/3)C_r(S_f/S_{delta} - .5S_{eff}/S_{delta}) \quad (3.24)$$

The center of pressure above is referenced to the leading edge at the root. In order to combine the fin center of pressure with the nose/body center of pressure it must be referenced to the same point. The nose/body center of pressure was easily referenced to the center of gravity since the tip of the nose is always at the origin of the coordinate system. The position of the fin's leading edge, however, will change everytime the root chord percentage or the radius of the projectile is changed. Foreshadowing the drag calculations of the next chapter, there will be a boattail on the projectile and the trailing edge of the fin will be at the start of the boattail. The boattail is set at ten percent of the body length so the leading edge of the fins referenced to the nose of the projectile will be at the total length of the projectile minus the root chord percentage plus ten percent. Subtracting the center of gravity location from the fin leading edge location will move the reference to the center of gravity frame. The center of pressure calculation for the fins becomes equation (3.25).

$$X_{CPf} = (2/3)C_r(S_f/S_{delta} - .5S_{eff}/S_{delta}) - [(1-(\%+.1))L_T-CG] \quad (3.25)$$

This center of pressure that relates the interference between the nose/body and fins and is found in graph (15) of Reference (2). As long as the tip chord does not become substantially shorter than the root chord and the span does not become substantially larger than the diameter of the projectile body equation (3.26) using a linear approximation of the graph will work.

$$X_{CPb} = -[\ C_r(.9988\beta(AR)+.35)] - [(1-(\%+.1))L_T-CG] \quad (3.26)$$

Graph (15) of Reference (2) once again is referenced to the root chord leading edge so the second factor is used to rereference the position to the center of gravity. If a configuration outside the limits above is desired the user will have to recalculate the above approximation using Reference (2) to meet their requirements.

4. Pitching Moment Coefficient

All the calculations above have been leading to the most important calculation. If the pitching moment coefficient, $C_{m\alpha}$, is negative there will be a restoring force acting against angle of attack changes to keep the projectile stable. The slope of the pitching moment coefficient in equation (3.27) is the combination of the quantities, most importantly the center of gravity referenced center of pressures, calculated above.

$$CM_\alpha = \{CN_\alpha X_{CPn} + [CN_{\alpha f}(X_{CPfb} K_{BW} + X_{CPf} K_{WB})S_f/2r]\}/2r \qquad (3.27)$$

C. RESULTS

The stability program, much like the configuration comparison program from the previous chapter, plots many different quantities against Mach number. Many more combinations are possible, should the user desire. The important plot for this thesis is the plot of the pitching moment coefficient as the Mach number is varied.

The projectile from Figure (1) with a long root chord, fourteen inches, and short span, about three quarters of an inch, and a five inch shaved side body with an ogive nose was modeled. This model produced the results presented in Figure (15) on the next page. Figure (15) shows that the slope of the pitching moment coefficient is indeed negative through the Mach region of interest, so there will be a restoring force against any angle of attack changes. An important distinction should be made here. The fins will help

Figure (15) CM alpha

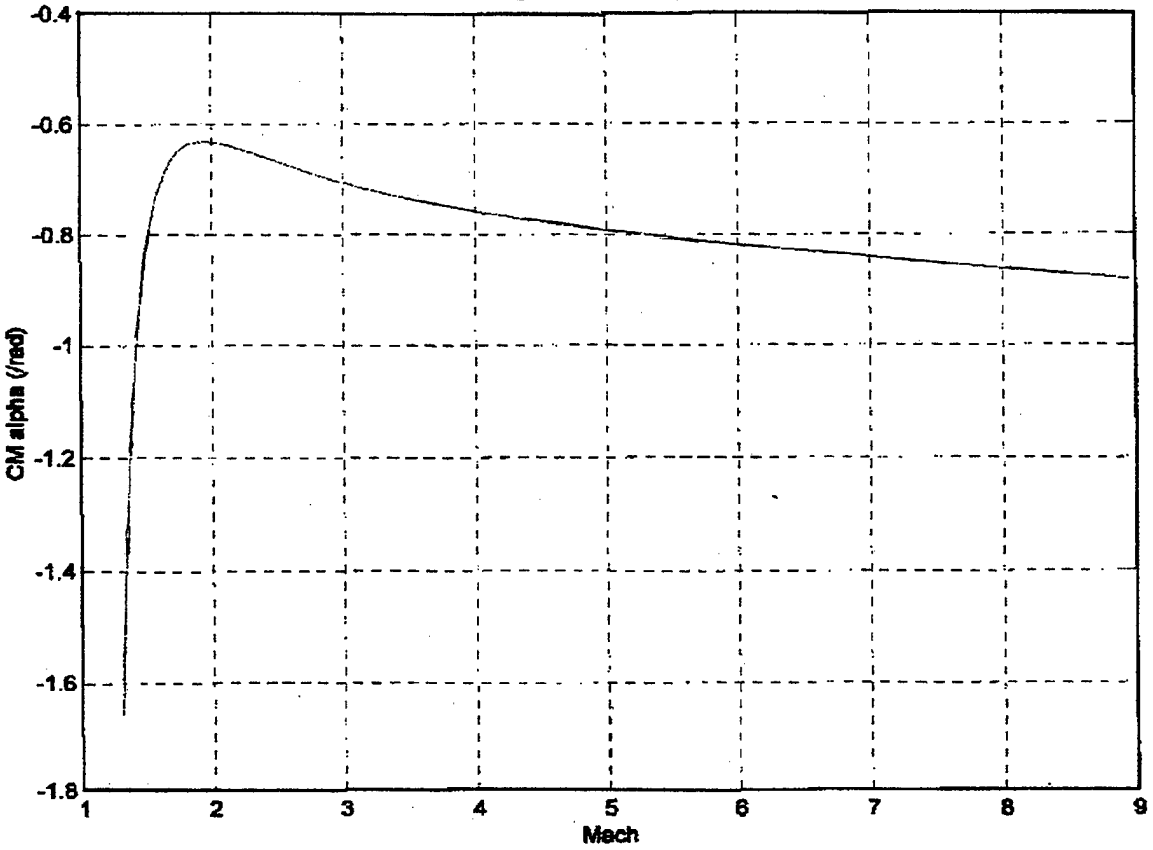

prevent the projectile from being tumbled by winds encountered in flight, but they will not prevent the projectile from being offset laterally by the wind, just like with conventional projectiles. The next chapter examines the trajectory of the projectile and depending on the angle of fire it is possible that the projectile may pass through the high winds of the jetstream. The speed of the jetstream winds, normally no higher than one hundred and fifty meters per second according to Reference (6), is small compared to the velocity of the projectile, normally no lower than one thousand meters per second at altitude. If the projectile were moving at its slowest and at ninety degrees to the maximum jet stream wind the angle of attack would only be eight degrees. The angle of attack change will be resisted by the fins, but the impact point of the projectile may be moved substantially.

IV. PERFORMANCE

The previous chapters have provided the physical dimensions of a stable projectile that meets the requirements of the rail gun concept. This chapter reviews the development of a program, written in the C computer language and provided in Appendix (B), to model the performance of the projectile.

A. PROJECTILE

Most of the dimensions of the projectile and fins are calculated with the equations from the configuration comparison and stability programs; translated into C for the performance program. There are, however, a couple of quantities not previously needed. The wetted area of the fins is used for the skin friction drag calculation and the base area is used for the base drag calculation.

The wetted area of the fins is determined by using the same assumptions that were used in determining the volume of the fins. The arc length at the mean aerodynamic chord is calculated using the radius of curvature of the fins and the angle as determined in Figure (6). The wetted surface area of the fins is the product of the radius of curvature, the angle subtended, the span, and by four to account for the four such surfaces that make up each fin. Equation (4.1) shows the formula using the same notation as in the fin volume calculation of the previous chapter.

$$S_{wf} = 4bR_f\theta_f \tag{4.1}$$

The base area of the projectile is the area at the very end of the projectile. The base area is reduced from the projectile's maximum cross sectional area because of the boattail. The boattail is set at eight degrees and as ten percent of the total body length. Reference (1) shows that these parameters provide the best performance at lower Mach

numbers which is where the projectile will spend the majority of its flight. The radius of curvature and the height of the rectangular area will be reduced by one tenth the total length multiplied by the tangent of eight degrees as shown in equations (4.2), (4.3), and (4.4).

$$r_{ba} = r - .014054L_T \tag{4.2}$$

$$\theta_{ba} = \pi/2 - \sin^{-1}(h/2r) \tag{4.3}$$

$$H_{ba} = r_{ba}\cos(\sin^{-1}(h/2r)) \tag{4.4}$$

Using equation (2.18) used for the projectile cross section, but with the reduced quantities from above, the surface area of the base can now be determined with equation (4.5).

$$S_{ba} = 2[(r_{ba})^2 \sin^{-1}(h/2r) - (r_{ba})^2\cos^2\theta_{ba}\cot\theta_{ba}] - 2hr_{ba}\cos(\sin^{-1}(h/2r)) \tag{4.5}$$

B. ATMOSPHERE

The drag force on the projectile is dependent on the projectile's environment. As the projectile moves through the atmosphere that environment changes, so the atmosphere, i.e., the environment, must be modeled. A standard atmosphere can be modeled as a series of linear temperature gradients and isotherms with increasing altitude as shown by reference (7). The temperature gradients, in degrees Kelvin are all of the form given in equation (4.6).

$$T = T_0 + ay/1000 \tag{4.6}$$

Where T_0 is the temperature at the bottom of the gradient in degrees Kelvin, a is the slope of the gradient in degrees Kelvin per meter, and y is the altitude in meters. As an example the T_0 is two hundred and eighty eight degrees Kelvin and the slope is minus six and a half from zero to eleven kilometers. The temperature is needed to determine the speed of sound and air density at each altitude.

The speed of sound, equation (4.7), at any altitude is the square root of gamma multiplied by the gas constant, R, for air and the temperature:

$$a = (\gamma RT)^{1/2} \tag{4.7}$$

The Mach number, used in the drag calculations below one hundred and five kilometers, is determined by dividing the projectile's velocity by the local (at altitude) speed of sound.

The skin friction drag of the projectile at altitude is directly proportional to air density at that particular altitude. The air density for any altitude is calculated in equation (4.8) as a percentage of sea level air density with the following equation:

$$\rho_a = \rho_{a0} (T/288)^{-[yg/R(T-288)]-1} \tag{4.8}$$

C. DRAG

The performance program uses six drag coefficients in determining the trajectory and impact velocity of the projectile. The skin friction drag and form drag coefficients for the nose/body and fins, and the base drag and boattail drag coefficients are calculated for the model.

1. Skin Friction Drag

The generic high velocity skin friction drag coefficient used in Chapter II is not sufficiently accurate for the performance calculations because of the larger range of velocities. The velocity varies from three thousand meter per second to as low as five hundred meters per second. The projectile's velocity is still the dominant factor in the numerator of the Reynold's number equation, equation (2.24) for the nose body and equation (4.9) for the fins.

$$Re_{n/b} = \rho v L_T/\mu \tag{2.24}$$

$$Re_f = \rho v C_{ma}/\mu \tag{4.9}$$

The skin friction drag coefficients calculated with equation (2.25), using the appropriate Reynolds number for the nose/body or fins, does not account for compressible flow at supersonic speeds.

$$C_f = .455\ [\mathrm{Log}_{10}(Re)]^{-2.58} \tag{2.25}$$

The compressible flow factor is calculated with equation (4.10).

$$f_{cf} = \{1 + [(\gamma-1)/2]M^2\}^{-.467} \tag{4.10}$$

Even with the compressible flow factor correction the skin friction coefficient is still close to .002. Even a small difference, however, over a long distance, can make a difference of kilometers in range, reducing the accuracy of the model.

The skin friction drag coefficients must be prepared for combination with the other drag coefficients for use in the equations of motion by multiplying them by the appropriate wetted area and dividing by the reference area, the projectile's maximum cross sectional area. These hybrid skin drag coefficients are the normal coefficients referenced to a common reference area in order simplify the computer programming and to facilitate the notation in this thesis. They are defined in equations (4.11) and (4.12).

$$C_{fb}' = C_{fb} f_{cf} (S_{no/s} + S_{bs})/S_{css} \tag{4.11}$$

$$C_{ff}' = C_{ff} f_{cf} S_{wf}/S_{css} \tag{4.12}$$

2. Form Drag

The form drag coefficients are determined by the methods from Reference (1). The form drag coefficient for the nose/body is calculated with the sane equations as in Chapter II.

$$C_{Fb} = (\Delta p/q)\{1-[(196(L_n/d)^2-16)/(14(M+18)(L_n/d)^2)]\} \tag{2.28}$$

$$\Delta p/q = [.083+(.096/M^2)](\sigma/10)^{1.69} \quad (2.29)$$

$$\sigma = \tan^{-1}(1/2f) \quad (2.30)$$

The form drag coefficient for the fins is equation (4.13).

$$C_{Ff} = (5.33\tau^2 S_f) / \beta(S_f - .5S_{eff}) \quad (4.13)$$

The biconvex configuration of the fins accounts for the 5.33. If a different wing configuration is desired, e.g. modified double wedge, the correct factor must be calculated by the user as shown in Reference (1) and changed in the equations of motion as this factor is not in the input section of the program. The terms S_f and S_{eff} are determined using equations (3.3) and (3.21) from Chapter III.

$$S_f = (C_r - C_t)b + 2C_t b \quad (3.3)$$

$$S_{eff} = S_f - \{[(1.1452\tan(\pi/2-\Lambda-\mu))/(\tan(\pi/2-\Lambda-\mu)+\tan(\Lambda-\pi/2-\mu))]^2 + [(1.1452\tan(\Lambda-\pi/2-\mu))/(\tan(\pi/2-\Lambda-\mu)+\tan(\Lambda-\pi/2-\mu))]^2\}\tan(\pi/2-\Lambda-\mu) \quad (3.21)$$

3. Boattail and Base Drag

The boattail drag, C_{bt}, and base drag, C_b, coefficients are empirical parameters presented graphically in Reference (1). Approximations are calculated in Appendix (D) with the other approximation formulas. The quantities coefficients determined by the approximations have to be adjusted to the reference area by dividing by the maximum projectile cross sectional area.

4. Drag Factor

The drag factor used in the equations of motion is a sum of the drag coefficients that have been referenced to the projectile's maximum cross sectional area multiplied by the dynamic head and reference area. Equation (4.14) presents the drag factor with the dynamic head shown in its component parts.

$$CD = (C_{fb}'+C_{ff}'+C_{Fb}+C_{Ff}+C_{bt}+C_b)S_{css}\rho v^2/2 \quad (4.14)$$

A review of the performance program will reveal that this equation never appears. The factors from the drag calculations and equations of motion are at times intermingled in the performance program in order to reduce the number of calculations and thus reduce the run time of the program.

D. EQUATIONS OF MOTION

The equations of motion in the performance program were originally written for an assignment in SE 4021 involving the super gun. SE 4021 is a computer simulation course in the Physics Department at the Naval Postgraduate School taught at the time by Dr. William Colson. The class assignment used a simple model of the atmosphere, a set projectile geometry, and a set drag coefficient based on a "bullet" shape. While this thesis went into far greater detail actually calculating those quantities, the actual equations of motion are not changed from the original assignment.

1. Velocity

The initial velocity is inputted by the user as the muzzle velocity. This velocity is decomposed into its lateral and vertical components in equations (4.15) and (4.16) by using the firing angle specified by the user as the initial angle of the trajectory, ϕ.

$$v_x = v\cos\phi \tag{4.15}$$

$$v_y = v\sin\phi \tag{4.16}$$

The performance program calculates the velocity at each time as a change from the previous time by a time step. The time step is calculated by dividing the muzzle velocity by the acceleration of gravity and multiplying by a user selected factor as in equation (4.17).

$$dt = .0001v/g \tag{4.17}$$

Determining the time step in this fashion allows the time step to be of reasonable length for the selected muzzle velocity. Using a small factor increases the number of time steps, which improves the accuracy of the model, but slows down the run time of the program.

The lateral and vertical velocities are calculated seperately with equations (4.18) and (4.19).

$$v_x(t) = v_x(t\text{-}dt) - kv(t\text{-}dt)v_x(t\text{-}dt)dt \tag{4.18}$$

$$v_y(t) = v_y(t\text{-}dt) - gdt - kv(t\text{-}dt)v_y(t\text{-}dt)dt \tag{4.19}$$

The vertical velocity is reduced not only by the effects of drag, but also by gravity. The non-subscripted velocity is the total velocity calculated with equation (4.20).

$$v = (v_x^2 + v_y^2)^{1/2} \tag{4.20}$$

The factor k is related to the factor CD, calculated in the previous section, by equation (4.21).

$$k = CD/mv^2 = (C_{fb}'+C_{ff}'+C_{Fb}+C_{Ff}+C_{bt}+C_b)S_{css}\rho/2m \tag{4.21}$$

Using k instead of CD in the equations of motion greatly simplifies the formulas. Dividing CD by m converts the drag force into an acceleration. Multiplying an acceleration by a time step provides a velocity. Dividing CD by the velocity squared is a contrivance to avoid having to track the angle of the trajectory at each time step. In equations (4.18) and (4.19) the v^2, which came from the dynamic head calculation, is replaced by $v(t)v_x(t\text{-}dt)$ and $v(t)v_y(t\text{-}dt)$, as appropriate, which have the angle information imbedded in the subscripted velocity as developed for the lateral case in equation (4.22).

$$v_x = v\cos\phi \;\; \therefore \; v^2\cos\phi = v(v\cos\phi) = vv_x \tag{4.22}$$

2. **Position**

The lateral and vertical positions are once again calculated separately with equations (4.23) and (4.24) by adding the change in position since the previous time step to the previous time step's position.

$$x(t) = x(t\text{-}dt) + v_x dt \tag{4.23}$$

$$y(t) = y(t\text{-}dt) + v_y dt \tag{4.24}$$

E. RESULTS

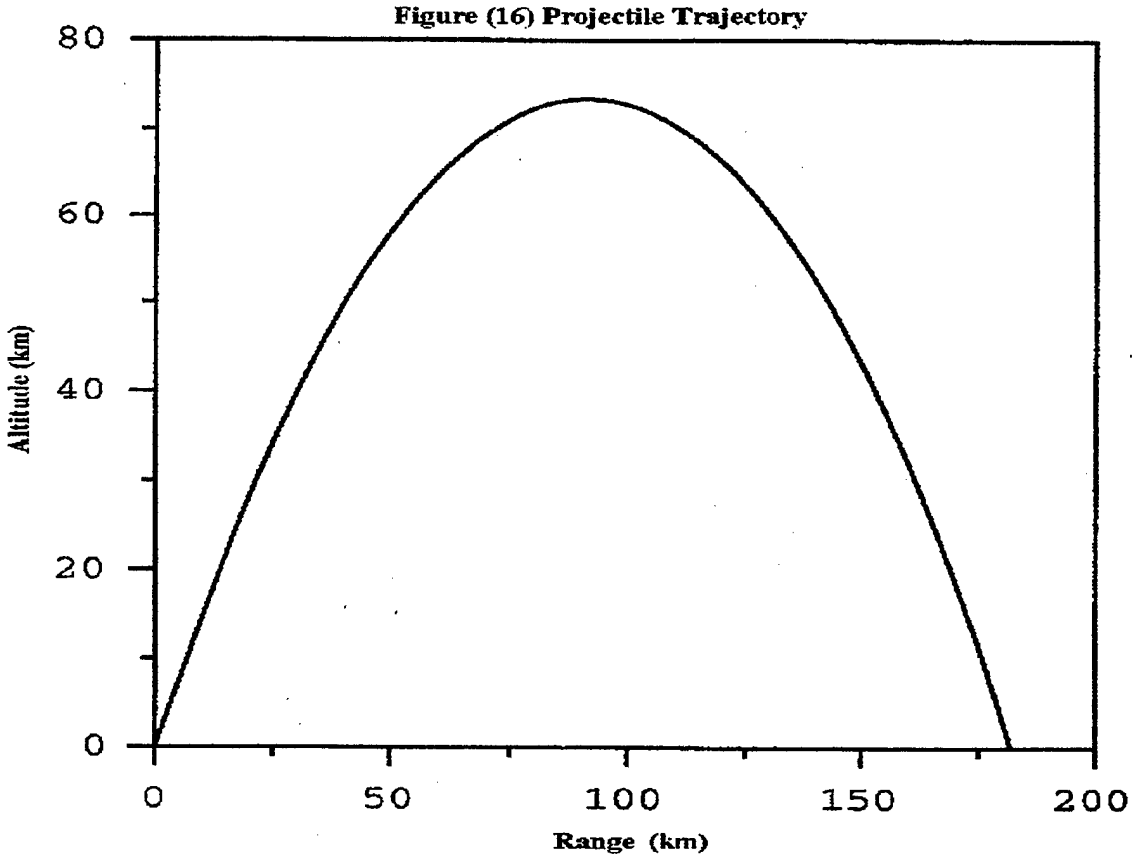

The projectile has a maximum range of one hundred and eighty two kilometers, as seen in Figure (16) above, when fired with a fifty seven degree launch angle. That range is approximately eight times the maximum range, twenty two kilometers, of a

conventional five inch gun. Figure (17) below shows that the projectile only takes four minutes and eight seconds to reach a target at its maximum range and eight seconds to reach a target at the maximum range of a conventional five inch gun.

Figure (17) Impact Time

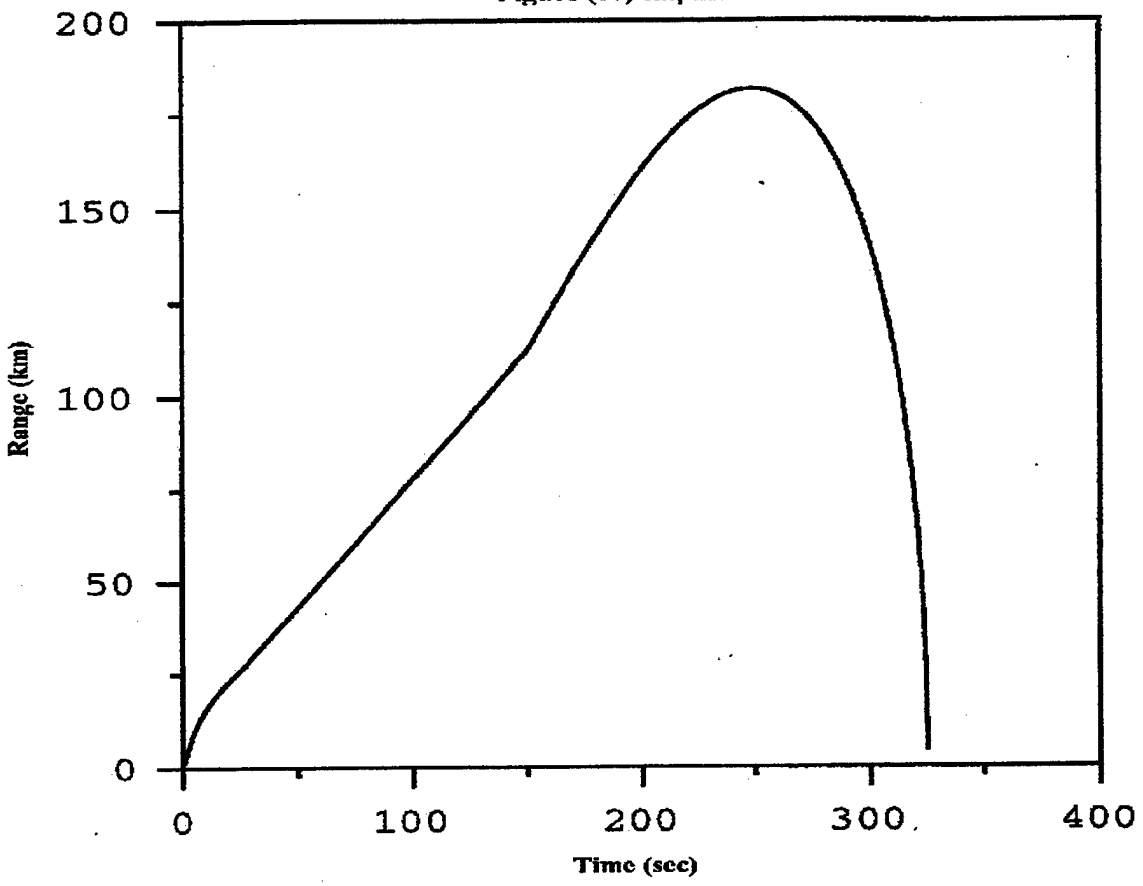

The kinetic energy of the projectile at impact is also substantially larger than a conventional five inch projectile. Figure (18) on the next page shows the energy of the projectile at impact for ranges from zero to maximum. There are two energies for almost all the ranges because the launch velocity is held constant and the launch angles are varied between zero and eighty nine and a half degrees. An interesting feature of Figure

(18) is that for ranges greater than sixteen kilometers the projectile has greater kinetic energy if shot at the high angle rather than the direct angle.

Figure (18) Kinetic Energy at Impact

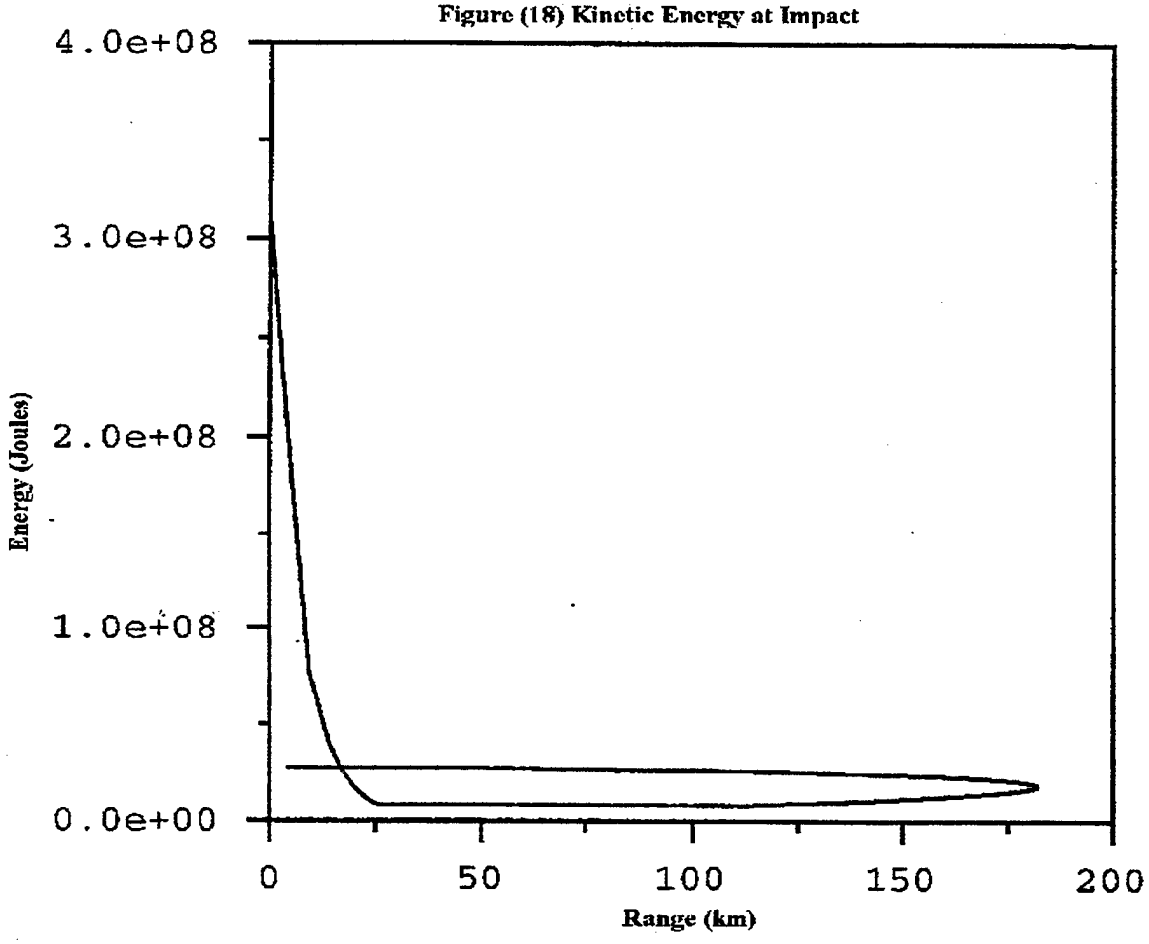

Two mechanisms are at work to improve the performance of the high angle shots. The first mechanism is that the high angle shots reach the higher atmosphere, which has lower density and thus less drag, quicker so they do not slow down as rapidly. The second mechanism is that the higher angle of fire shots also descend at a higher angle so gravity helps recoop some of the drag loss, i.e. the vertical component of velocity is a larger part of the total velocity.

Some of the points of interest on Figure (18) are the maximum energy, the energy crossover point between direct fire and high angle fire, the minimum energy, and the energy at maximum range. At the muzzle of the rail gun the projectile has a maximum kinetic energy of three hundred and seven megajoules, this is equivalent to the energy released by detonating two hundred and forty four pounds of TNT. The crossover point where the kinetic energy of a projectile fired at a shallow angle (direct fire) and a high angle occurs at about sisteen kilometers. The kinetic energy at sixteen kilometers is twenty seven megajoules, this is equivalent to twenty one pounds of TNT. Referring to Figure (17), the projectile takes either eleven or three hundred and twenty five seconds to arrive. The minimum kinetic energy of six point eight megajoules, equivalent to only five and a half pounds of TNT, occurs at fifty kilometers with a launch angle of twenty one and a half degrees. The projectile reaches fifty kilometers in one minute. As mentioned above the projectile reaches its maximum range of one hundred and eighty two kilometers in four minutes and eight seconds. The projectile has eighteen magajoules of kinetic energy when it impacts at its maximum range, this energy is equivalent to fifteen pounds of TNT.

The projectile often has the kinetic energy equivalent to an amount of TNT substantially larger than the explosive payload of the projectile. The destructive power, however, may be substantially less than the TNT because there is no mechanism to efficiently transfer the projectile's kinetic energy to the target.

V. CONCLUSIONS AND RECOMMENDATIONS

An aerodynamically stable projectile can be made for a rectangular barrel. Figure (1) shows the basic configuration and dimensions of the projectile developed and then used as an example in this thesis. The projectile performs very well, but the performance model is for the best expected muzzle velocity and with a mass that may be too large for practical shipboard deployment. The real benefit of this thesis is the three computer programs that will allow future users to quickly analyze different projectile configurations to meet evolving requirements.

A great deal can be done to improve the capabilities of the programs developed in this thesis. The development and incorporation of the equations for the subsonic regime into the models, with a transsonic approximation to link the subsonic and supersonic regimes, will allow a greater variety of materials to be considered. Different fin types, i.e. double wedge or modified double wedge, can also be incorporated into the models to give users a choice.

A proper heat transfer study of the projectile should be done. The information from a heat transfer study can be used to determine both the fineness ratio at which the ogive nose would melt and what materials can be used in the construction of the projectile. The form drag of the nose is dependent on the fineness ratio. The performance of the projectile can be improved by making the nose pointier to reduce the drag, but if the nose is too pointy it may melt. Different materials may be used for different portions of the projectile if the temperature of a desired component is known not to exceed the melting point of the components constituent material.

Wind tunnel testing could verify the drag equations used or provide information to improve their accuracy. Hypersonic wind tunnels are very expensive to operate, but the proposed projectile flies most of its trajectory at velocities easily achieved in standard wind tunnels. A study of the true effects of the flat contact surfaces would determine if the assumptions made in calculating the drag of the projectile's body sufficiently accounted for the airflow separation and turbulence that the flat contact surfaces will probably cause.

The most difficult study required may well be determining what explosive compound to use in the projectile and how it can be fused. The explosive compound used will have to be able to undergo the shock of the rapid acceleration experienced in the barrel of the rail gun and the high temperatures the projectile may reach without detonating. Electrical fuses may be damaged, or worse, detonated by the very high currents encountered in the barrel. An impact fuse in the base may work, but a thorough study should be done to insure the projectile does not detonate in the barrel of the rail gun.

Experiments with rail guns are on going. This thesis provides tools to help in the design of the total weapon system.

APPENDIX (A) MATLAB MODEL FOR NOSE/BODY CONFIGURATION COMPARISON

```
% Inputs

stin=.5;  % skin thickness in inches
rhos=19200.0;  % density of metal in kg/m^3 (tungsten)
rhoe=1520.0;  % density of explosive in kg/m^3 (C4)
v0=3000; % initial shell velocity in m/s
cwin=2;  % width of contact area in inches
ew=5.5;  % explosive weight in kg
f=1;  %  fineness ratio, (nose length)/diameter

% Constants

rho=1.03; % air density at sea level in kg/m^3
a=346; % speed of sound in air at seal level/standard day in m/s

% Calculated Initial Values

M0=v0/a;
q=.5*rho*(v0^2); % kg/m-s^2
stm=stin*.025416;  % skin thickness in meters
cwm=cwin*.025416;  % width of contact area in meters

% Drag Factors

Cf=.002; % skin friction drag coefficient from AA3710 notes pg 6-4
sigmasph=45; % semivertex angle in degree for sphere
sigmaogi=57.2958*atan(1/(2*f)); % semivertex angle in degrees for ogive
presssph=(.083+(.096/(M0^2)))*((sigmasph/10)^1.69);
      % from AA3710 notes pg 12-2
pressogi=(.083+(.096/(M0^2)))*((sigmaogi/10)^1.69);
CDFsph=presssph*(1-(((392*(.5^2))-32)/(26*(M0+18)*(.5^2))));
CDFogi=pressogi*(1-(((392*(f^2))-32)/(26*(M0+18)*(f^2))));

% Spherical with Wedge Insert

srinw=Linspace(2,6,30); % radius in inches
sdinw=(2.*srinw)+cwin; % Projectile width in inches
srmw=srinw*.0254166667; % radius in meters
snvw=(((2/3)*pi).*(srmw.^3))+(((pi/2)*cwm).*(srmw.^2));
      % Nose volume in m^3
snww=rhos.*snvw; % Weight of nose in kilograms
spcsw=(pi.*(srmw.^2))+((2*cwm).*srmw);
      % Projectile cross section in meters^2
spcsiw=spcsw./.000646; % Projectile cross section in in^2
secsw=(pi.*((srmw-stm).^2))+((2*cwm).*(srmw-stm));
      % Explosives cross section in m^2
selw=ew./(rhoe.*secsw); % Length of explosive in meters
spwkw=(rhos.*(((spcsw-secsw).*selw)+(stm.*spcsw)))+ew+snww;
      % Projectile weight in kilograms
spwlw=spwkw.*2.2; % Projectile weight in lbm
stlmw=srmw+selw+stm; % Total length of projectile in meters
```

```
stliw=stlmw/.0254166667; % Total length in inches
ssamw=(2.*pi.*(srmw.^2))+(pi.*srmw.*cwm)+(2.*pi.*srmw.*(selw+stm))...
   +(2.*(selw+stm).*cwm);  % Projectile Surface Area in m^2
ssaiw=ssamw./.000646; % Projectile Surface Area in in^2
ssfdmw=Cf*ssamw*q; % skin friction drag
sfdmw=CDFsph*spcsw*q; % form drag

% Spherical with Shaved Sides

srins=Linspace(2.0,6,30); % radius in inches
sdins=(2.*srins); % Projectile width in inches
srms=srins*.0254166667; % radius in meters
snvs=(((2/3)*pi).*(srms.^3))-((cwm.*(srms.^2)*pi.*.5)-...
   (cwm.*(srms.^2).*acos(cwm./(4.*srms)))-(4.*(srms.^3).*(sqrt(1-...
   (((cwm./(4.*srms)).^2)))))+(4.*(srms.^3))-((srms.*cwm./24).*...
   ((cwm./(2.*sin(acos(cwm./(16.*srms))))))+(cwm./(2.*sin(acos(cwm./...
   (8.*srms)))))+(3.*cwm./(2.*sin(acos((3.*cwm)./(16.*srms)))))+...
   (cwm./(2.*sin(acos(cwm./(4.*srms)))))))+((cwm./(96.*srms)).*...
   (((cwm.^3)./(128.*sin(acos(cwm./(16.*srms))))))+((cwm.^3)./(32.*...

sin(acos(cwm./(8.*srms)))))+((27.*(cwm.^3))./(128.*sin(acos((3.*cwm)...
   ./(16.*srms)))))+((cwm.^3)./(8.*sin(acos(cwm./(4.*srms)))))));
      % Nose volume in m^3
snws=rhos.*snvs; % Weight of nose in kilograms
spcss=(pi.*(srms.^2))-(2.*(((srms.^2).*((pi/2)-...
   acos(.5*cwm./srms)))-(((srms-(srms.*(1-
sin(acos(.5.*cwm./srms)))))...
   .^2).*cot(acos(.5*cwm./srms)))));
      % Projectile cross section in meters^2
spcsis=spcss./.000646; % Projectile cross section in in^2
secss=(pi.*((srms-stm).^2))-(2.*((((srms-stm).^2).*((pi/2)-...
   acos(.5*cwm./(srms-stm))))-((((srms-stm)-((srms-stm).*...
   (1-sin(acos(.5.*cwm./(srms-stm)))))).^2).*...
   cot(acos(.5*cwm./(srms-stm))))));  % Explosives cross section in m^2
sels=ew./(rhoe.*secss); % Length of explosive in meters
spwks=(rhos.*(((spcss-secss).*sels)+(stm.*spcss)))+ew+snws;
      % Projectile weight in kilograms
spwls=spwks.*2.2; % Projectile weight in lbm
stlms=srms+sels+stm; % Total length of projectile in meters
stlis=stlms/.0254166667; % Total length in inches
ssams=(2.*pi.*(srms.^2))-(2.*pi.*(((-(srms.^2)./2).*log((.5.*cwm)+...
   sqrt((srms.^2)+(.25.*(cwm^2))))))+(.25.*cwm.*sqrt((srms.^2)+(.25.*...
   (cwm^2))))+(.5.*(srms.^2).*log(srms))))+(pi.*((cwm.*.5).^2))+...
   (4.*srms.*(sels+stm).*asin(.5.*cwm./srms))+(2.*cwm.*(sels+stm));
      % Projectile Surface Area in m^2
ssais=ssams./.000646; % Projectile Surface Area in in^2
ssfdms=Cf*ssams*q; % skin friction drag
sfdms=CDFsph*spcss*q; % form drag


% Ogival with Wedge Insert

orinw=Linspace(2,6,30); % radius in inches
odinw=(2.*orinw)+cwin; % Projectile width in inches
ormw=orinw.*.0254166667; % radius in meters
onlw=2.*ormw.*f; % nose length in meters
oRmw=((onlw.^2)+(ormw.^2))./(2.*ormw);
```

```
      % Radius of curvature of nose in meters
thetaw=acos(onlw./oRmw);
onvw=(pi.*((onlw.*((2.*(oRmw.^2))-(2.*oRmw.*ormw)+(ormw.^2)))-...
   ((onlw.^3)./3)-(onlw.*(oRmw-ormw).*sqrt((oRmw.^2)-(onlw.^2)))...
   -((oRmw-ormw).*(oRmw.^2).*asin(onlw./oRmw))))+(cwm.*(((oRmw.^2)...
   .*((pi/2)-thetaw))-(((oRmw-ormw).^2).*cot(thetaw))));
   % Nose volume in m^3
onww=rhos.*onvw; % Weight of nose in kilograms
opcsw=(pi.*(ormw.^2))+(2.*cwm.*ormw);
      % Projectile cross section in meters^2
opcsiw=opcsw./.000646; % Projectile cross section in in^2
oecsw=(pi.*((ormw-stm).^2))+(2.*cwm.*(ormw-stm));
      % Explosives cross section in m^2
oelw=ew./(rhoe.*oecsw); % Length of explosive in meters
opwkw=(rhos.*(((opcsw-oecsw).*oelw)+(stm.*opcsw)))+ew+onww;
      % Projectile weight in kilograms
opwlw=opwkw.*2.2; % Projectile weight in lbm
otlmw=(f.*2.*ormw)+oelw+stm; % Total length of projectile in meters
otliw=otlmw/.0254166667; % Total length in inches
osamw=(2.*pi.*((2.*f.*ormw.*oRmw)-(oRmw.*(oRmw-ormw).*asin...
   (2.*f.*ormw./oRmw))))+(2.*cwm.*oRmw.*((pi/2)-thetaw))+...
   (2.*pi.*ormw.*(oelw+stm))+(2.*cwm.*(oelw+stm));
      % Projectile Surface Area in m^2
osaiw=osamw./.000646; % Projectile Surface Area in in^2
osfdmw=Cf*osamw*q; % skin friction drag
ofdmw=CDFogi*opcsw*q; % form drag


% Ogival with Shaved Sides

orins=Linspace(2.0,6,30); % radius in inches
odins=(2.*orins); % Projectile width in inches
orms=orins*.0254166667; % radius in meters
onls=2.*orms.*f; % nose length in meters
oRms=((onls.^2)+(orms.^2))./(2.*orms);
      % Radius of curvature of nose in meters
thetas=acos(onls./oRms);
onvs=(pi.*((onls.*((2.*(oRms.^2))-(2.*oRms.*orms)+(orms.^2)))-...
   ((onls.^3)./3)-(onls.*(oRms-orms).*sqrt((oRms.^2)-(onls.^2)))...
   -((oRms-orms).*(oRms.^2).*asin(onls./oRms))))-((cwm.*(oRms.^2)*...
   pi.*.5)-(cwm.*(oRms.^2).*acos((f.*cwm)./(2.*oRms)))-((2./f).*...
   (oRms.^3).*(sqrt(1-(((f.*cwm)./(2.*oRms)).^2))))+((2.*(oRms.^...
   3))./f)-((f.*oRms.*cwm./12).*((cwm./(2.*sin(acos((f.*cwm)./(8.*...
   oRms)))))+(cwm./(2.*sin(acos((f.*cwm)./(4.*oRms))))))+(3.*cwm./...
   (2.*sin(acos((3.*f.*cwm)./(8.*oRms))))))+(cwm./(2.*sin(acos((f.*...
   cwm)./(2.*oRms)))))))+(((cwm.*(f.^3))./(12.*oRms)).*(((cwm.^3)./...
   (128.*sin(acos((f.*cwm)./(8.*oRms))))))+((cwm.^3)./(32.*sin(acos...
   ((f.*cwm)./(4.*oRms))))))+((27.*(cwm.^3))./(128.*sin(acos((3.*f.*...

cwm)./(8.*oRms))))))+((cwm.^3)./(8.*sin(acos((f.*cwm)./(2.*oRms)))))));
      % Nose volume in m^3
onws=rhos.*onvs; % Weight of nose in kilograms
opcss=(pi.*(orms.^2))-(2.*(((orms.^2).*((pi/2)-acos(.5*cwm./orms)))-...
   (((orms-(orms.*(1-sin(acos(.5.*cwm./orms))))).^2).*cot(acos(.5.*...
   cwm./orms)))));
      % Projectile cross section in meters^2
opcsis=opcss./.000646; % Projectile cross section in in^2
```

```
oecss=(pi.*((orms-stm).^2))-(2.*((((orms-stm).^2).*((pi/2)-...
   acos(.5*cwm./(orms-stm))))-((((orms-stm)-((orms-stm).*...
   (1-sin(acos(.5.*cwm./(orms-stm))))))).^2).*...
   cot(acos(.5*cwm./(orms-stm))))));  % Explosives cross section in m^2
oels=ew./(rhoe.*oecss); % Length of explosive in meters
opwks=(rhos.*(((opcss-oecss).*oels)+(stm.*opcss)))+ew+onws;
      % Projectile weight in kilograms
opwls=opwks.*2.2; % Projectile weight in lbm
otlms=(f.*2.*orms)+oels+stm; % Total length of projectile in meters
otlis=otlms/.0254166667; % Total length in inches
osams=(2.*pi.*((2.*f.*orms.*oRms)-(oRms.*(oRms-orms).*asin...
   (2.*f.*orms./oRms))))-(oRms.*((pi.*cwm)-(2.*cwm.*acos((f.*cwm)./...
   (2.*oRms)))-((4.*oRms.*sqrt(1-(((f.*cwm)./(2.*oRms)).^2))).*f)+...
   (4.*oRms./f)))+(2.*(((oRms.^2).*((pi./2)-acos(cwm./oRms)))-...
   (((oRms-(cwm/2)).^2).*cot(acos(cwm./oRms)))))+(4.*orms.*(oels+...
   stm).*asin(.5.*cwm./orms))+(2.*cwm.*(oels+stm));
      % Projectile Surface Area in m^2
osais=osams./.000646; % Projectile Surface Area in in^2
osfdms=Cf*osams*q; % skin friction drag
ofdms=CDFogi*opcss*q; % form drag

figure(1)
plot(sdinw,spcsiw,'k-',sdins,spcsis,'k.'),grid
title('Cross Section vs Width')
xlabel('Projectile Width (in)'),ylabel('Projectile Cross Section
(in^2)')
text(6.1,110,'Solid = w/ Insert')
text(6.1,105,'Dotted = w/ Shaved Sides')
figure(2)
plot(sdinw,spwlw,'k-',sdins,spwls,'k.',odinw,opwlw,'k.-.',odins,...
   opwls,'k--'),grid
title('Weight vs Width')
xlabel('Projectile Width (in)'), ylabel('Projectile Weight (lbm)')
text(6.1,654,'Solid = Spherical w/ Insert')
text(6.1,614,'Dotted = Spherical w/ Shaved Sides')
text(6.1,574,'Dash/Dot = Ogival w/ Insert')
text(6.1,534,'Dashed = Ogival w/ Shaved Sides')
figure(3)
plot(sdinw,stliw,'k-',sdins,stlis,'k.',odinw,otliw,'k.-.',odins,...
   otlis,'k--'),grid
title('Length vs Width')
xlabel('Projectile Width (in)'), ylabel('Total Length (in)')
text(6.1,41,'Solid = Spherical w/ Insert')
text(6.1,38.5,'Dotted = Spherical w/ Shaved Sides')
text(6.1,36,'Dash/Dot = Ogival w/ Insert')
text(6.1,33.5,'Dashed = Ogival w/ Shaved Sides')
figure(4)
plot(spwlw,stliw,'k-',spwls,stlis,'k.',opwlw,otliw,'k.-.',opwls,...
   otlis,'k--'),grid
title('Length vs Weight')
xlabel('Projectile Weight (lbm)'), ylabel('Total Length (in)')
text(205,41,'Solid = Spherical w/ Insert')
text(205,38.5,'Dotted = Spherical w/ Shaved Sides')
text(205,36,'Dash/Dot = Ogival w/ Insert')
text(205,33.5,'Dashed = Ogival w/ Shaved Sides')
figure(5)
plot(spwlw,spcsiw,'k-',spwls,spcsis,'k.',opwlw,opcsiw,'k.-.',opwls,...
```

```
   opcsis,'k--'),grid
title('Cross Section vs Weight')
xlabel('Projectile Weight (lbm)'),ylabel('Projectile Cross Section
(in^2)')
text(215,37,'Solid = Spherical w/ Insert')
text(215,30,'Dotted = Spherical w/ Shaved Sides')
text(215,23,'Dash/Dot = Ogival w/ Insert')
text(215,16,'Dashed = Ogival w/ Shaved Sides')
figure(6)
plot(spcsiw,ssaiw,'k-',spcsis,ssais,'k.',opcsiw,osaiw,'k.-.',opcsis,...
   osais,'k--'),grid
title('Surface Area vs Cross Section')
xlabel('Projectile Cross Section (in^2)')
ylabel('Projectile Surface Area (in^2)')
text(21,480,'Solid = Spherical w/ Insert')
text(21,460,'Dotted = Spherical w/ Shaved Sides')
text(21,440,'Dash/Dot = Ogival w/ Insert')
text(21,420,'Dashed = Ogival w/ Shaved Sides')
figure(7)
plot(ssfdmw,sfdmw./1e5,'k-
',ssfdms,sfdms./1e5,'k.',osfdmw,ofdmw./1e5,...
   'k.-.',osfdms,ofdms./1e5,'k--'),grid
title('Form Drag vs Skin Friction Drag at Sea Level, V0=3000 km/s')
xlabel('Skin Friction Drag (kg-m/s^2)'),ylabel('Form Drag  x 100,000
(kg-m/s^2)')
text(1750,1.56,'Solid = Spherical w/ Insert')
text(1750,1.41,'Dotted = Spherical w/ Shaved Sides')
text(1750,1.26,'Dash/Dot = Ogival w/ Insert')
text(1750,1.11,'Dashed = Ogival w/ Shaved Sides')
figure(8)
plot(sdinw,ssfdmw,'k-',sdins,ssfdms,'k.',odinw,osfdmw,'k.-.',odins,...
   osfdms,'k--'),grid
title('Skin Friction Drag vs Width at Sea Level, V0=3000 km/s')
xlabel('Projectile Width (in)'),ylabel('Skin Friction Drag (kg-m/s^2)')
text(6.1,2900,'Solid = Spherical w/ Insert')
text(6.1,2800,'Dotted = Spherical w/ Shaved Sides')
text(6.1,2700,'Dash/Dot = Ogival w/ Insert')
text(6.1,2600,'Dashed = Ogival w/ Shaved Sides')
figure(9)
plot(sdinw,sfdmw./1e5,'k-',sdins,sfdms./1e5,'k.',odinw,ofdmw./1e5,...
   'k.-.',odins,ofdms./1e5,'k--'),grid
title(Form Drag vs Width at Sea Level, V0=3000 km/s')
xlabel('Projectile Width (in)'),ylabel('Form Drag/100,000 (kg-m/s^2)')
text(5,2.41,'Solid = Spherical w/ Insert')
text(5,2.24,'Dotted = Spherical w/ Shaved Sides')
text(5,2.07,'Dash/Dot = Ogival w/ Insert')
text(5,1.90,'Dashed = Ogival w/ Shaved Sides')
```

If a color printer is available different colored lines are a better presentation on the plots.

APPENDIX (B) PERFORMANCE PROGRAM (in C)

```
/*Performance*/
#include <stdio.h>
#include <math.h>
main(){
      float g,C,rhoo,rho,A,v,vx,vy,x,y,theta,t,dt,k,h,xf,yf,pi,r,f;
      float a,M,T,Reb,Ref,CDFb,Cfb,CDfb,pr,gamma,R,mu,SA,pb,dc,dce,er;
      float CDbt,CDb,nb,lb,Sb,rin,stin,rhom,rhoe,stm,nl,nv,nw,br,lbt;
      float ecs,el,ew,nlm,nlm2,nlm3,tlm,l,sigma,ein,r2,r3,sigmac,cwin;
      float cr,ct,lamdam,mac,tau,tmac,rf,phi,bin,b,fv,fw,fsa,m,cw3;
      float ibrh,ibrw,omega,pf,Cff,CDff,CDFf,beta,Mu,seff,sf,et,nbt;
      float lamda,psi,Psi,D1,D2,D3,comf,rn,rn2,rn3,thetan,crp,f3,cw;
      int j;

      /* INPUTS */
      rin=2.5; /* radius in inches */
      stin=.5; /* skin thickness in inches */
      cwin=2; /* width of contact area in inches */
      rhom=19200.0;
        /* density of metal in kg/m^3 (tungsten in example) */
      rhoe=1520.0;
       /* density of explosive in kg/m^3 (C4 in this example) */
      ew=5.5; /* desired explosive payload in kg */
      v=3000.0; /* muzzle velocity in m/s */
      theta=.986111; /* launch angle in radians (56.5 degrees) */
      tau=.03; /* fin thickness to chord ratio */
      crp=.6; /* fin percentage of total body length */
      lamda=.585686; /* leading edge sweep angle */
      f=1; /* nose fineness ratio, (nose length)/(body diameter) */

      /* CONSTANTS */
      rhoo=1.03; /* air density at sea level in kg/m^3 */
      pi=3.141593;
      g=9.81; /* gravity in m/s^2 */
      gamma=1.4; /* gamma for air */
      R=287; /* gas constant for air in SI units*/
      mu=1.8e-5; /* coefficient of viscosity */
      a=340.17;
            /* Speed of sound at sea level on standard day in m/s */

      /* INITIAL VALUES */
      x=0.0; /* initial position */
      y=0.0; /* initial altitude */
      t=0.0; /* initial time */
      j=0; /* counter variable */

      /* CALCULATED INITITIAL VALUES AND CONSTANTS */
      vx=v*cos(theta); /* initial lateral velocity in m/s */
      vy=v*sin(theta); /* initial vertical velocity in m/s */
      M=v/a; /* Mach Number for muzzle velocity at sea level */

      /* Projectile Dimensions and Parameters */
      r=rin*.025417; /* radius in meters */
      r2=r*r;
      r3=r*r*r;
```

```
      stm=stin*.025417; /* skin thickness in meters */
      cw=cwin*.025417; /* width of contact area in meters */
      cw3=cw*cw*cw;
      nl=f*2*rin; /* nose length in inches */
      nlm=f*2*r; /* nose length in m */
      nlm2=nlm*nlm;
      nlm3=nlm*nlm*nlm;
      rn=((nlm*nlm)+r2)/(2*r); /*radius of curviture of nose in m */
      rn2=rn*rn;
      rn3=rn*rn*rn;
      thetan=acos(nlm/rn); /* angle of arc swept by nose */
      ein=rin-stin; /* explosive radius in inches */
      er=ein*.025417; /* explosive radius in meters */
      f3=f*f*f;
      nv=(pi*((nlm*((2*rn2)-(2*rn*r)+r2))-(nlm3/3)-((rn-r)*nlm*
            sqrt(rn2-nlm2))-((rn-r)*rn2*asin(nlm/rn))))-((cw*rn2*
pi*.5)-(cw*rn2*acos((f*cw)/(2*rn)))-((2/f)*rn3*sqrt(1-
      (((f*cw)/(2*rn))*((f*cw)/(2*rn)))))+((2*rn3)/f)-((f*rn*
cw/12)*((cw/(2*sin(acos((f*cw)/(8*rn)))))+(cw/(2*sin
(acos((f*cw)/(4*rn)))))+(3*cw/(2*sin(acos((3*f*cw)/
(8*rn)))))+(cw/(2*sin(acos((f*cw)/(2*rn))))))+(((cw*f3)/
(12*rn))*((cw3/(128*sin(acos((f*cw)/(8*rn)))))+(cw3/
(32*sin(acos((f*cw)/(4*rn)))))+((27*cw3)/(128*sin(acos
((3*f*cw)/(8*rn)))))+(cw3/(8*sin(acos((f*cw)/(2*rn)))))));
            /* nose volume in m^3 */
      nw=rhom*nv; /* nose mass in kilograms */
      A=(pi*r2)-(2*((r2*((pi/2)-acos(.5*cw/r)))-(((r-(r*(1-sin(acos
          (.5*cw/r)))))*(r-(r*(1-sin(acos(.5*cw/r))))))*(.5*cw/r)*
          (1/sin(acos(.5*cw/r))))));
            /* projectile cross section in m^2 */
      ecs=(pi*((r-stm)*(r-stm)))-(2*((((r-stm)*(r-stm))*((pi/2)-acos
          (.5*cw/(r-stm))))-((((r-stm)-((r-stm)*(1-sin(acos(.5*cw/
          (r-stm))))))*((r-stm)-((r-stm)*(1-sin(acos(.5*cw/
          (rstm))))))*(.5*cw/(r-stm))*(1/sin(acos(.5*cw/(r-
          stm)))))));
            /* explosives cross section in m^2 */
      el=ew/(rhoe*ecs); /* length of explosive in m */
      tlm=nlm+el+stm; /* total length of projectile in m */
      l=(5*r*(1-sin(acos(2/(5*rin))))); /* intermediate calculation */
      SA=(2*pi*((2*f*r*rn)-(rn*(rn-r)*asin(2*f*r/rn))))-(rn*((pi*cw)-
          (2*cw*acos((f*cw)/(2*rn)))-((4*rn*sqrt(1-(((f*cw)/(2*rn))
          *((f*cw)/(2*rn)))))/f)+(4*rn/f)))+(2*((rn2*((pi/2)-acos
          (cw/rn)))-(((rn-(cw/2))*(rn-(cw/2)))*(cw/rn)*(1/sin(acos
          (cw/rn))))))+(4*r*(el+stm)*asin(.5*cw/r))+(2*cw*(el+stm));
              /* projectile surface area in m^2 */
      sigma=(360*atan(rin/nl))/pi;
        /* semivertex angle at ogive point in degrees */
      br=r-(tlm*.014054);
       /* base r in m w/ 8 deg boatail .1 the length of projectile */
          omega=(pi/2)-asin(cw/(2*r));
 /* half angle of base's curved section */
      ibrh=br*cos(omega); /* intermediate step */
      ibrw=br*cos((pi/2)-omega); /* intermediate step */
      Sb=(2*((br*br*((pi/2)-omega))-(ibrh*ibrh*(cos(omega)
          /sin(omega)))))+(2*cw*ibrw); /* base area in m^2 */
      cr=crp*tlm; /* root chord in meters */
      psi=(pi/2)-lamda; /* "inside" sweep angle of leading edge */
```

```
b=2*((sqrt(2*((r*sin(acos(.5*cw/r)))*(r*sin(acos
      (.5*cw/r))))))-r);  /* span of single fin in meters */
ct=(cr-(.5*b/tan(psi))); /* tip chord in meters */
Psi=pi-psi; /* "inside sweep" angle of tip */
sf=(.5*b*(cr-ct))+(ct*b); /* planform area of fin pair in m^2 */
lamdam=ct/cr; /* intermediate calculation */
mac=(.666667*cr*(1+lamdam+(lamdam*lamdam)))/(1+lamdam);
      /* mean aerodynamic chord in meters */
tmac=mac*tau; /* fin thickness at MAC in meters */
rf=mac*(1+(tau*tau))/(4*tau);
      /* radius of curviture of biconvex fins at MAC in meters */
phi=(pi/2)-asin(mac/(2*rf));
      /* lower limit of integration for quarter of fin volume */
fv=2*b*(((rf*rf)*((pi/2)-phi))-(((rf*rf)-(rf*tmac)+(.25*tmac
      *tmac))*cos(phi)/sin(phi)));
         /* volume of single fin in m^3 */
fw=2*rhom*fv; /* mass of all four fins in kg */
fsa=16*rf*((pi/2)-phi)*b; /* surface area of four fins */
m=(rhom*(((A-ecs)*el)+(stm*A)))+ew+nw+fw
  /* projectile mass in kg */
dt=.0001*(v/g); /* time step for integration */

printf("%f,%f,%f,%f,%f\n",x/1000,y/1000,v,t,M);
while(y>=0 && y<11000){
      T=288-((6.5*y)/1000);/* Adiabatic Cooling w/ Alt Increase*/
      a=sqrt(gamma*R*T);
      dc=((y*g)/(R*(T-288.16)))+1;
      dce=pow((T/288.16),-dc);
      rho=rhoo*dce;
      v=sqrt(vx*vx+vy*vy);
      M=v/a;
      beta=sqrt((M*M)-1);
      Mu=asin(1/M);
      D1=tan(psi-Mu);D2=tan(Psi-Mu);D3=D1+D2;
       /* intermediate calcs */
      Reb=(rho*v*tlm)/mu; /* Reynolds number for body */
      Ref=(rho *v*mac)/mu; /* Reynolds number for fins */
      pb=pow((log(Reb)/log(10)),-2.58);
      pf=pow((log(Ref)/log(10)),-2.58);
      Cfb=.455*pb; /*Yellow book*/
      Cff=.455*pf;
      comf=pow((1+(((gamma-1)/2)*M*M)),-.467);
      /* compressible flow factor */
      CDfb=(Cfb*SA*comf)/A;
      CDff=(Cff*fsa*comf)/A;
      sigmac=pow((sigma/10),1.69);
      pr=sigmac*(.083+(.096/(M*M)));
      CDFb=pr*(1-(((196*f*f)-16)/(14*(M+18)*(f*f))));
      seff=sf-(((1.1452*D1/D3)*(1.1452*D1/D3)*D2)+
            ((1.1452*D2/D3)*(1.1452*D2/D3)*D1));
      CDFf=(5.33*tau*tau*(sf-(.5*seff)))/(beta*sf);
      lbt=500000*((.0555*M*M)+(.006*M)+(-.00255*M*M*M)+.85);
      nbt=((-485*M)*(-485*M))-(lbt);
      CDbt=(10*((485*M)-sqrt(nbt))/250000)-.00375;
      lb=4000*((.007*M*M)+(.00007*M)+(-.0009*M*M*M)+.85);
      nb=((-445*M)*(-445*M))-(lb);
      CDb=110*Sb*((445*M)-sqrt(nb))/(2000*A);
```

```
            C=CDfb+CDff+CDFb+CDFf+CDbt+CDb;
            k=(C*rho*A)/(2*m);
            vx=vx-(k*v*vx*dt);
            vy=vy-g*dt-(k*v*vy*dt);
            x=x+vx*dt;y=y+vy*dt;t=t+dt;
            j=j+1;
            if(j>=100){
                  printf("%f,%f,%f,%f,%f\n",x/1000,y/1000,v,t,M);
                  j=0;}}
      while(y>=11000 && y<25000){
            Isothermal Region
            Equations of Motion Loop}
      while(y>=25000 && y<47000){
            T=216.5+(3*(y-25000)/1000); /* Adiab. Heating w/ Alt Inc*
            Equations of Motion Loop}
      while(y>=47000 && y<53000){
            Isothermal Region
            Equations of Motion Loop}
      while(y>=53000 && y<79000){
            T=282.5-(4.5*(y-53000)/1000); /* Adiab. Cooling w/ Alt
Inc*/
            Equations of Motion Loop}
      while(y>=79000 && y<=90000){
            Isothermal Region
            Equations of Motion Loop}
      while(y>=90000 && y<=105000){
            T=165.5+(4*(y-90000)/1000); /* Adiab. Heating w/ Alt Inc*/
            Equations of Motion Loop}
      while(y>=105000){Drag is Effectively Zero Above this Altitude so
            all the drag calculations are removed from the loop and the
            drag terms are removed from the equations of motion}
      while(y>=90000){
            Isothermal Region
            T=165.5+(4*(y-90000)/1000); /* Adiab. Cooling w/ Alt Dec*/
            Equations of Motion Loop}
      while(y>=79000){
            Isothermal Region
            Equations of Motion Loop}
      while(y>=53000){
            T=282.5-(4.5*(y-53000)/1000);/* Adiab. Heating w/ Alt Dec*/
            Equations of Motion Loop}
      while(y>=47000){
            Isothermal Region
            Equations of Motion Loop}
      while(y>=25000){
            T=216.5+(3*(y-25000)/1000); /* Adiab. Cooling w/ Alt Dec*/
            Equations of Motion Loop}
      while(y>=11000){
            Isothermal Region
            Equations of Motion Loop}
      while(y>=0){
            T=288-((6.5*y)/1000); /* Adiabatic Heating w/ Alt Dec*/
            Equations of Motion Loop}
      xf=x-((vx*y)/vy);
      yf=y-((vy*y)/vy);
      printf("%f,%f,%f,%f,%f\n",xf/1000,yf/1000,v,t,M);}
```

APPENDIX (C) MATLAB STABILITY PROGRAM

```
% Stability Study

% Inputs
r=2.5; % projectile radius in inches
h=2; % width of contact area in inches
f=1; % nose fineness ratio
st=.5;  % skin thickness in inches
rhos=19200.0;  % density of metal in kg/m^3 (tungsten)
rhoe=1520.0;  % density of explosive in kg/m^3 (C4)
ew=5.5;  % explosive weight in kg
tau=0.03; % fin thickness ratio
z=.6; % root chord/total length

% Constants
gamma=1.40;
rho=.00004; % air density in lbm/cubic inch
T=520; % Standard temperture at sea level in Rankine
a=(sqrt(gamma*32.2*53.3*T))*12; % Speed of sound in inches/second

% Nose/Body
d=(2*r); % Projectile width in inches
rm=r*.0254166667; % radius in meters
hm=h*.0254166667; % width of contact areas in meters
stm=st*.0254166667; % skin thickness in meters
nl=2*rm*f; % nose length in meters
nli=2*r*f; % nose length in inches
Rm=((nl^2)+(rm^2))/(2*rm);
      % Radius of curvature of nose in meters
thetas=acos(nl/Rm);
nv=(pi*((nl*((2*(Rm^2))-(2*Rm*rm)+(rm^2)))-((nl^3)/3)-(nl*(Rm-rm)*...
   sqrt((Rm^2)-(nl^2)))-((Rm-rm)*(Rm.^2)*asin(nl/Rm))))-((hm*(Rm^2)*...
   pi*.5)-(hm*(Rm^2)*acos((f*hm)/(2*Rm)))-((2/f)*(Rm^3)*(sqrt(1-...
   (((f*hm)/(2*Rm))^2))))+((2*(Rm^3))/f)-((f*Rm*hm/12)*((hm/(2*sin...
   (acos((f*hm)/(8*Rm))))))+(hm/(2*sin(acos((f*hm)/(4*Rm))))+(3*hm./...

(2*sin(acos((3*f*hm)/(8*Rm))))+(hm/(2*sin(acos((f*hm)/(2*Rm))))))+...
   (((hm*(f^3))/(12*Rm))*(((hm^3)/(128*sin(acos((f*hm)/(8*Rm))))))+...
   ((hm^3)/(32*sin(acos((f*hm)/(4*Rm))))))+((27*(hm^3))/(128*sin(acos...
   ((3*f*hm)/(8*Rm))))))+((hm^3)/(8*sin(acos((f*hm)/(2*Rm))))))));
      % Nose volume in m^3
nw=rhos.*nv; % Weight of nose in kilograms
pcs=(pi*(rm^2))-(2*(((rm^2)*((pi/2)-acos(.5*hm/rm)))-(((rm-(rm*(1-
sin...
   (acos(.5*hm/rm))))))^2)*cot(acos(.5*hm/rm))));
      % Projectile cross section in meters^2
pcsi=pcs/.000646; % Projectile cross section in in^2
ecs=(pi*((rm-stm).^2))-(2*((((rm-stm)^2)*((pi/2)-acos(.5*hm/(rm-
stm))))-...
   ((((rm-stm)-((rm-stm)*(1-sin(acos(.5*hm/(rm-stm))))))^2)*cot(acos...
   (.5*hm/(rm-stm))))));  % Explosives cross section in m^2
      % Explosives cross section in m^2
```

```
el=ew/(rhoe*ecs); % Length of explosive in meters
eli=el/.025416667; % Length of explosive in inches
pwk=(rhos*(((pcs-ecs)*el)+(stm*pcs)))+ew+nw;
      % Projectile weight in kilograms
pwl=pwk*2.2; % Projectile weight in lbm
tlm=(f*2*rm)+el+stm; % Total length of projectile in meters
tli=tlm/.0254166667; % Total length in inches
sam=(2*pi*((2*f*rm*Rm)-(Rm*(Rm-rm)*asin(2*f*rm/Rm))))-(Rm*((pi*hm)-
(2*...
   hm*acos((f*hm)/(2*Rm)))-((4*Rm*sqrt(1-(((f*hm)/(2*Rm))^2)))/f)+...
   (4*Rm/f)))+(2*(((Rm^2)*((pi/2)-acos(hm/Rm)))-(((Rm-(hm/2))^2)*cot...
   (acos(hm/Rm)))))+(4*rm*(el+stm)*asin(.5*hm/rm))+(2*hm*(el+stm));
      % Projectile Surface Area in m^2
sai=sam./.000646; % Projectile Surface Area in in^2

%fins
b=2*((sqrt(2*((r*sin(acos(.5*h/r)))^2)))-r); % span in inches w/o body
bm=b*.025416667; % span in meters
cr=z*tli;   % centerline chord in inches
lamda=.585686;
% sweep ang. of 34 deg(in rads); keeps LE supersonic down to Mach 1
theta=(pi/2)-lamda; % "inside" sweep angle of 56 degrees
ct=(cr-(.5*b/tan(theta)));   % tip chord in inches
Sf=(.5*b*(cr-ct))+(ct*b);     % planform area of fin pair in square
inches
Sd=(cr^2)*tan(theta);   % area if delta where whole in sqare inches
S1=Sf/Sd;
S2=Sf/pcsi;
mac=(2*cr*(1+(ct/cr)+((ct/cr)^2)))/(3*(1+(ct/cr)));
% mean aerodynamic chord of fins in inches
macm=mac*.025416667; % mean aerodynamic chord of fins in meters
Rmf=(((.5*mac)^2)+((.5*tau*mac)^2))/(tau*mac);
% radius of curviture of biconvex fin at mac in inches
Rmfm=Rmf*.0254166667;
      % radius of curviture of biconvex fin at mac in meters
thetaf=acos(.5*mac/Rmf);
fw=2*rhos*bm*(((Rmfm^2)*((pi/2)-thetaf))-(((Rmfm-(.5*tau*macm))^2)...
   *cot(thetaf))); % Weight of single fin in kg
phi=pi-theta; % "inside" tip angle of 129 degrees
AR=b^2/Sf;
K1=5.33;
Apri=2*tau/3;

% Center of Gravity
tw=pwk+(2*fw); % weight of entire projectile including fins in kg
CGn=.707*nli*nw; % CG point for the nose
CGb=((.5*eli)+nli)*((rhos*(pcs-ecs)*el)+ew); % CG point for body
CGep=((.5*st)+eli+nli)*(stm*pcs*rhos); % CG point for the end plate
CGf=((mac*.5)+((1-(z+.1))*tli))*2*fw;
CG=(CGn+CGb+CGep+CGf)/tw; % CG point of projectile

% Interference Factors
rs=r/(r+(b/2));
Kbf=(.869*((rs+.65)^2))-.367;
Kfb=(.278*((rs+1.3)^2))+.529;
kbf=rs;
kfb=(.2*((rs-.5)^2))+.95;
```

```
M=linspace(1.3,9,250);
beta=sqrt(M.^2-1);
mu=asin(1./M);
if (beta./f)<=1
   CNan=(-.28.*(((beta./f)-1.9).^2))+3.58;
   % Approximation over Mach range for chart pg 13-4
   Xn=CG-(tli.*((.125.*beta./f)+.15));
   % From graph pg 14-8 adjusted to CG
else
   CNan=(-3.4.*(((f./beta)-.9).^2))+3.4;
   Xn=CG-(tli.*((-.125.*f./beta)+.425));
end
D1=tan(theta-mu);
D2=tan(phi-mu);
D3=D1+D2;
if ((b/2)-((cr+ct).*tan(mu)))<=0
   Seff=Sf-((((1.1452.*D1./D3).^2).*D2)+(((1.1452.*D2./D3).^2).*D1));
   % Effected tip area (split into two terms to account for overlap)
else
   Seff=((cr^2).*tan(mu))+((ct^2).*tan(mu));
end
CNa2df=(4./beta);
% CNalpha before tip effects
CNaf=CNa2df-((2.*Seff)./(beta.*Sf));
CNa=CNan+(CNaf.*(Kbf+Kfb).*S2);
CNd=CNaf.*((kbf+kfb)*S2);
Xf=-(cr*.666666*(S1-(.5.*Seff./Sd)))-(((1-(z+.1))*tli)-CG);
% CP of fin adjusted for missing area and to CG
Xbf=-(cr.*((.9888.*beta.*AR)+.35))-(((1-(z+.1))*tli)-CG);
% From NACA figure 15i and adjusted to CG
CMa=((CNan.*Xn)+(CNaf.*(((Xbf.*Kbf)-(Xf.*Kfb)).*S2))./d;
CM1=CMa.*.017453;
CM3=CMa.*.052360;
CM5=CMa.*.087227;
CM10=CMa.*.174533;
CMd=(CNaf.*((Xbf.*kbf)+(Xf*kfb))*S2)./d; %From pg 20-2
q=.5.*rho.*((a.*M).^2);
CN=pwl./(q.*pcsi);
atrim=((CN.*CMd)./((CNa.*CMd)+(CNd.*CMa))).*57.3;
LFS=(CNd).*q.*pcsi./pwl;
cpn=Xn./d;
cpf=Xf./d;


figure(1),plot(M,CNa,'k'),grid
title('CN alpha'),xlabel('Mach'),ylabel('CN alpha (/rad)')
figure(2),plot(M,CNd,'k'),grid
title('CN delta'),xlabel('Mach'),ylabel('CN delta (/rad)')
figure(3),plot(M,CMa,'k'),grid
title('CM alpha'),xlabel('Mach'),ylabel('CM alpha (/rad)')
figure(4),plot(M,CMd,'k'),grid
title('CM delta'),xlabel('Mach'),ylabel('CM delta (/rad)')
figure(5),plot(M,atrim,'k'),grid
title('Alpha trim'),xlabel('Mach'),ylabel('Alpha trim (deg)')
figure(6),plot(M,LFS,'k'),grid
```

```
title('Load Factor Sensitivity'),xlabel('Mach'),ylabel('(n-1)/delta')
figure(7),plot(M,CNan,'k'),grid
title('Cnalpha Nose/Body Alone'),xlabel('Mach'),ylabel('CNalpha
(/rad)')
figure(8),plot(M,CNaf,'k'),grid
title('Cnalpha Fin Alone'),xlabel('Mach'),ylabel('CNalpha (/rad)')
figure(9),plot(M,cpn,'k'),grid
title('Xcp Nose/Body'),xlabel('Mach'),ylabel('Xcp(from cg)/body
diameter')
figure(10),plot(M,cpf,'k'),grid
title('Xcp Fin'),xlabel('Mach'),ylabel('Xcp(from cg)/body diameter')
figure(11),plot(M,CM1,'k'),grid
title('CM at One Degree'),xlabel('Mach'),ylabel('CM')
figure(12),plot(M,CM3,'k'),grid
title('CM at Three Degrees'),xlabel('Mach'),ylabel('CM')
figure(13),plot(M,CM5,'k'),grid
title('CM at Five Degrees'),xlabel('Mach'),ylabel('CM')
figure(14),plot(M,CM10,'k'),grid
title('CM at Ten Degrees'),xlabel('Mach'),ylabel('CM')
```

APPENDIX (D) Graph Approximation Programs

The first program provided approximates the four interference factors.

```
% Interference Factors

clear
rs=linspace(0,1,20);

%KBW
A=.869;
B=.65;
C=-.367;
KBW=(A.*((rs+B).^2))+C;

%kBW
kBW=rs;

%KWB
A=.278;
B=1.3;
C=.529;
KWB=(A.*((rs+B).^2))+C;

%kWB
A=.2;
B=-.5;
C=.95;

kWB=(A.*((rs+B).^2))+C;
figure(1)
plot(rs,KBW,'k',.2,.279,'ok',.4,.607,'ok',.6,1,'ok',.8,1.446,'ok',...
   rs,kBW,'k',.2,.213,'dk',.4,.41,'dk',.6,.61,'dk',.8,.8,'dk',...
   rs,KWB,'k',.2,1.16,'*k',.4,1.35,'*k',.6,1.55,'*k',.8,1.77,'*k'),grid
hold
plot(rs,kWB,'k',.2,.958,'^k',.4,.933,'^k',.6,.94,'^k',.8,.967,'^k')
title('Interference Factors')
xlabel('Radius to Semispan Ratio')
text(.43,1.5,'KWB')
text(.64,1.3,'KBW')
text(.21,.91,'kWB')
text(.41,.35,'kBW')
```

Figure(19) on the next page is the plot of this program.

Figure (19) Interference Factors

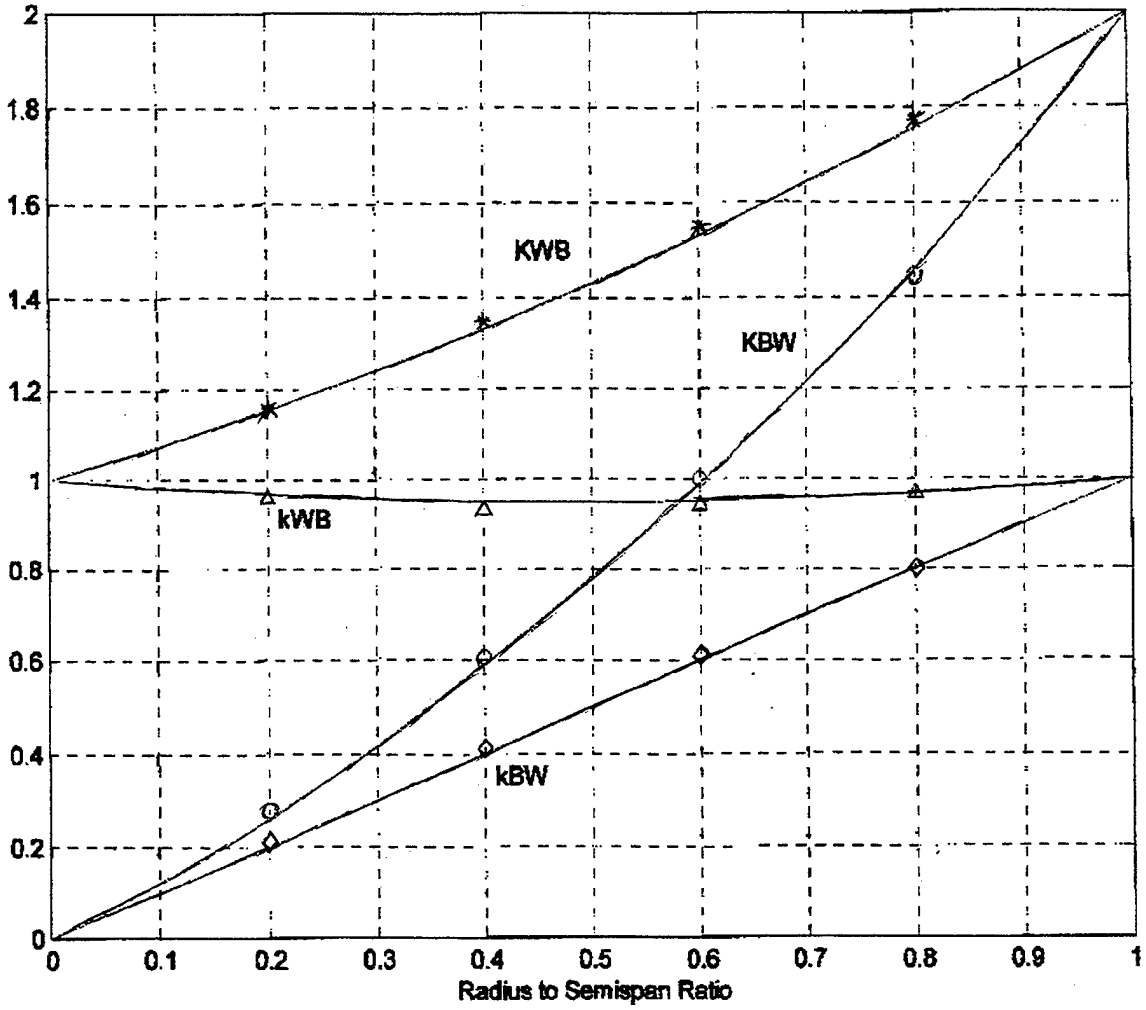

The nose/body lift coefficient is calculated by two programs. The curve changes when the the fineness ratio equals β and the two branches needed to be done seperately.

```
% Nose-Body CNalpha Graphic Approximation

% Left side of USAF DATCOM figure 4.2.1.1-5a on pg 13-4 of AA3701 notes

A=-.28;
B=-1.9;
C=3.58;
Beta=linspace(.4,1,100);
CNalpha=(A.*((Beta+B).^2))+C;
figure(1)
plot(Beta,CNalpha,'k',.4,2.95,'ko',.6,3.1,'ko',.8,3.25,'ko',1,3.35,'ko'
),grid
title('CNalpha vs Beta/fN')
xlabel('Beta divided by Nose Length/Body Diameter ratio')
ylabel('Cnalpha')


% Nose-Body CNalpha Graphic Approximation
% Right side of USAF DATCOM figure 4.2.1.1-5a on pg 13-4 of AA3701
notes

A=-3.4;
B=-.9;
C=3.4;
Beta=linspace(.1118,1,100);
CNalpha=(A.*((Beta+B).^2))+C;
figure(1)
plot(Beta,CNalpha,'k',.5,2.86,'ko',.6,3.09,'ko',.8,3.36,'ko',.9,3.4,'ko
',...
   1,3.35,'ko'),grid
title('CNalpha vs Beta/fN')
xlabel('Beta divided by Nose Length/Body Diameter ratio')
ylabel('Cnalpha')
```

Figure (20) and Figure (21) on the next two pages are the plots of these two programs.

Figure (20) Normal Force Coefficient for Nose/Body Combination

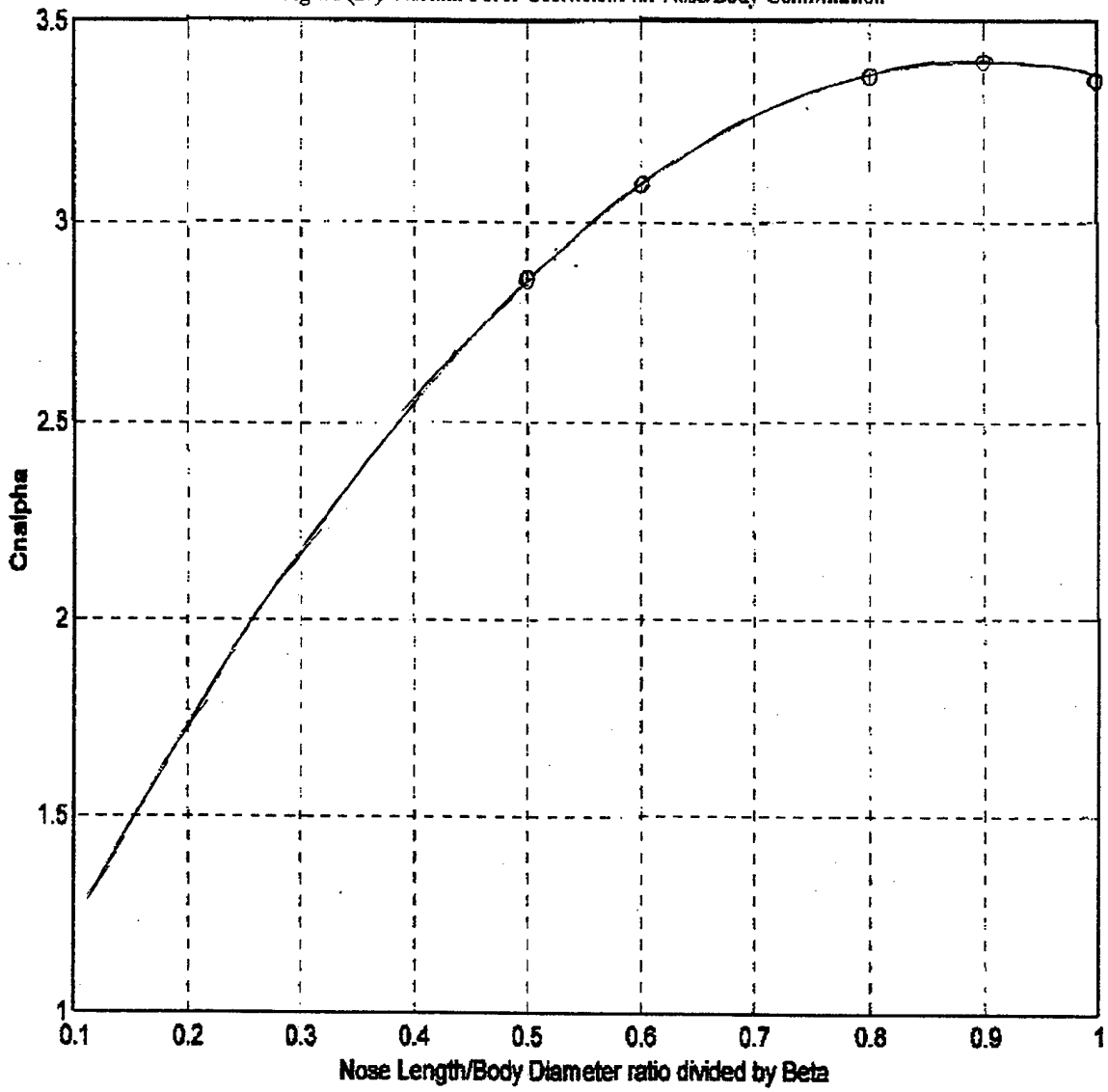

Figure (21) Normal Force Coefficient for Nose/Body Combination

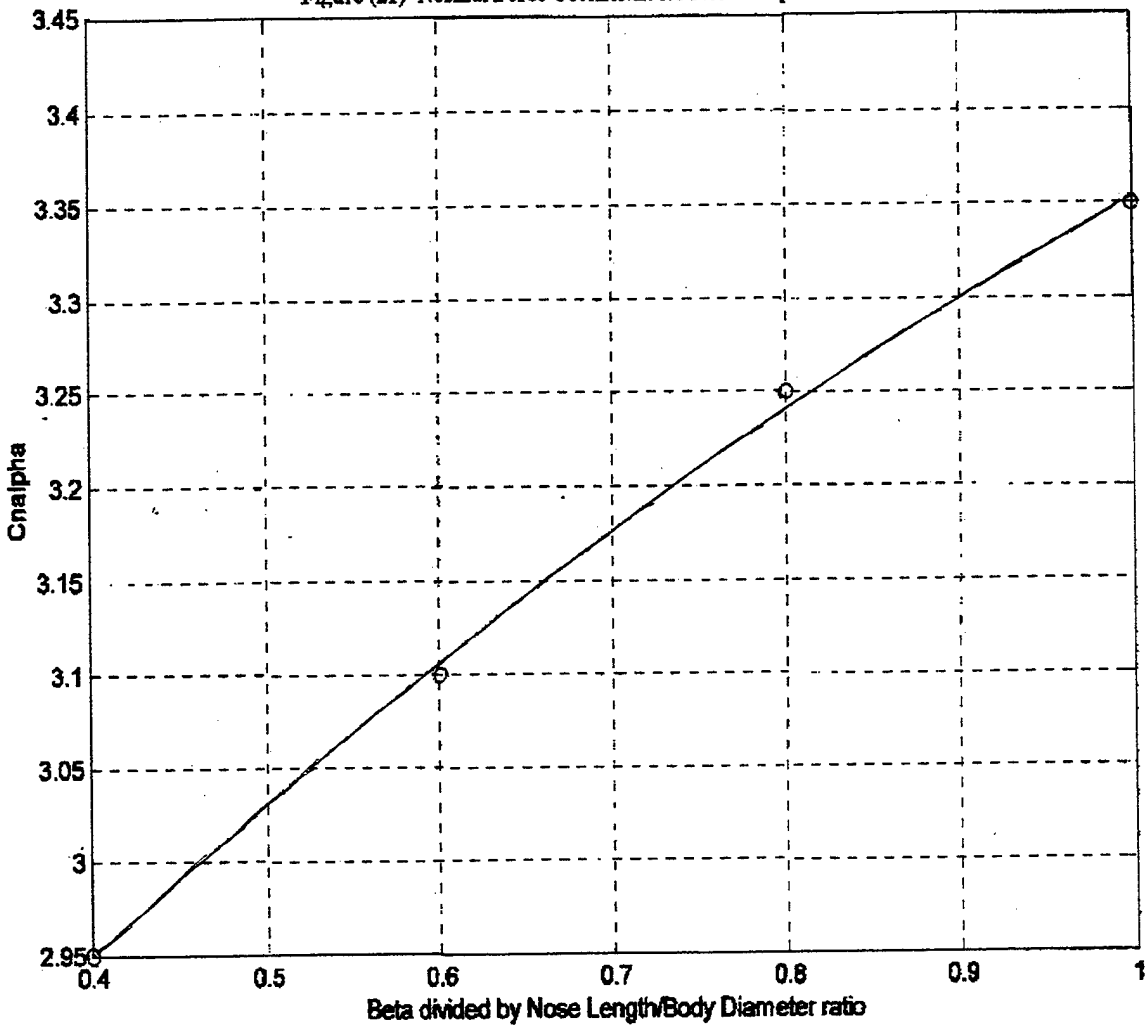

The boattail drag and base drag coefficients are calculated from the following graphs.

```
A=-2000;
B=65000;
C=.69;
D=-570;
E=1;
F=.0115;
G=-.00097;
M=linspace(1.2,9,100);
m=((D.*M).^2)-(4.*B.*((C.*M)+(F.*(M.^3))+(G.*(M.^4))+E));
cd=(10.*(-(D.*M)-sqrt(m))./(2*B))-.015;
figure(1)
plot(M,cd,'k',1.5,.0171,'ko',2,.01,'ko',2.5,.0071,'ko',3,.0057,'ko',...
   3.5,.0054,'ko',4,.0051,'ko'),grid
title('Boattail Drag Coefficient vs Mach Number')
xlabel('Mach Number'),ylabel('Boattail Drag Coefficient')


% Base Pressure Coefficient Graphic Approximation
% From Chin pg 31
A=.007;
B=1000;
C=.00007;
D=-445;
E=.85;
F=-.0009;
M=linspace(1,9,100);
m=((D.*M).^2)-(4.*B.*((A.*(M.^2))+(C.*M)+(F.*(M.^3))+E));
cd=110.*(-(D.*M)-sqrt(m))./(2*B);
figure(1)
plot(M,cd,'k',1.2,.168,'ko',1.4,.148,'ko',1.8,.12,'ko',2.2,.1,'ko',2.6,
.082,...
   'ko',3.0,.072,'ko'),grid
title('Base Pressure Coefficient vs Mach Number')
xlabel('Mach Number'),ylabel('Base Pressure Coefficient')
```

The plots are presented as Figure (22) and Figure (23) on the next two pages.

Figure (22) Boattail Drag Coefficient vs Mach Number

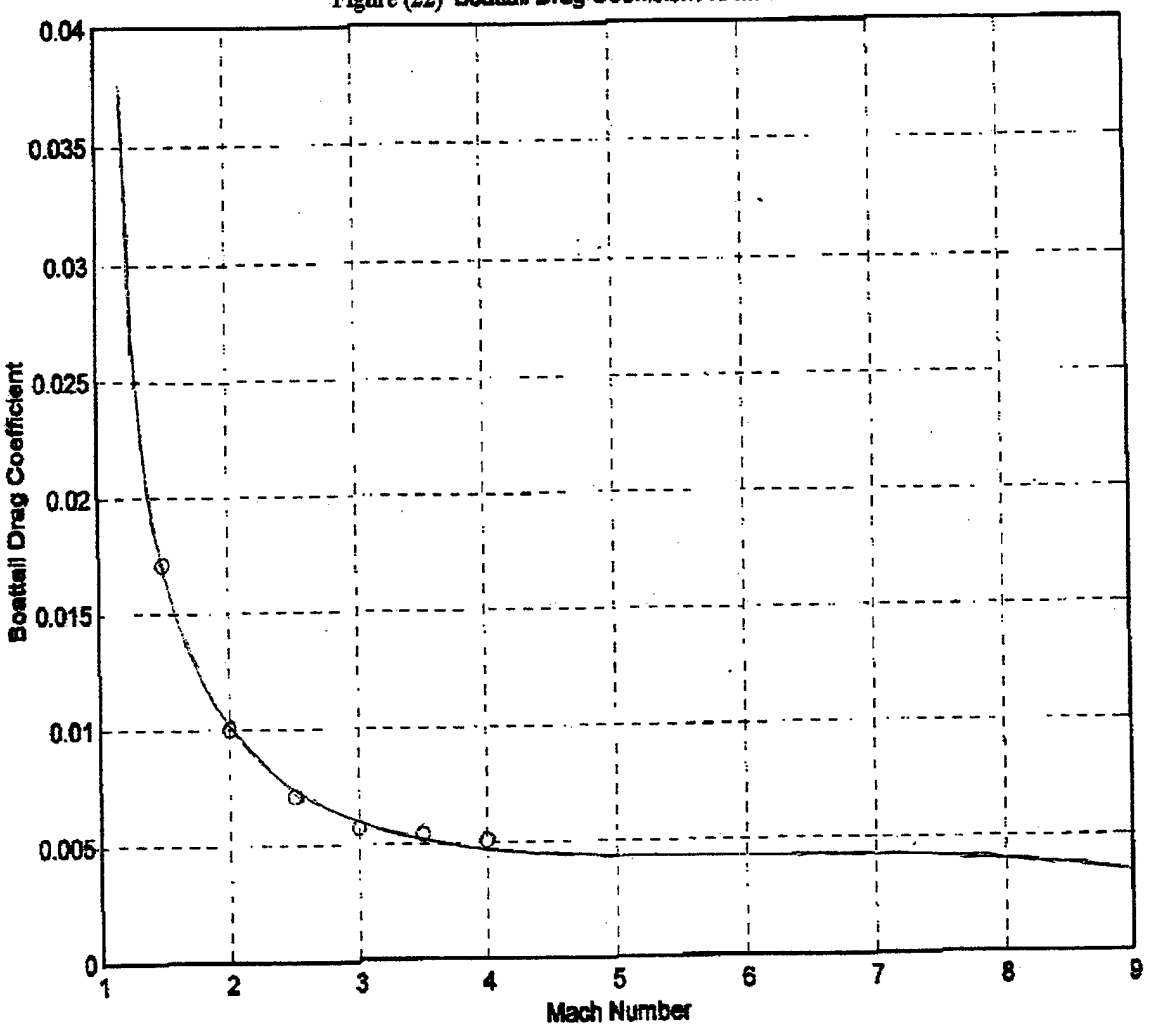

Figure (23) Base Pressure Coefficient vs Mach Number

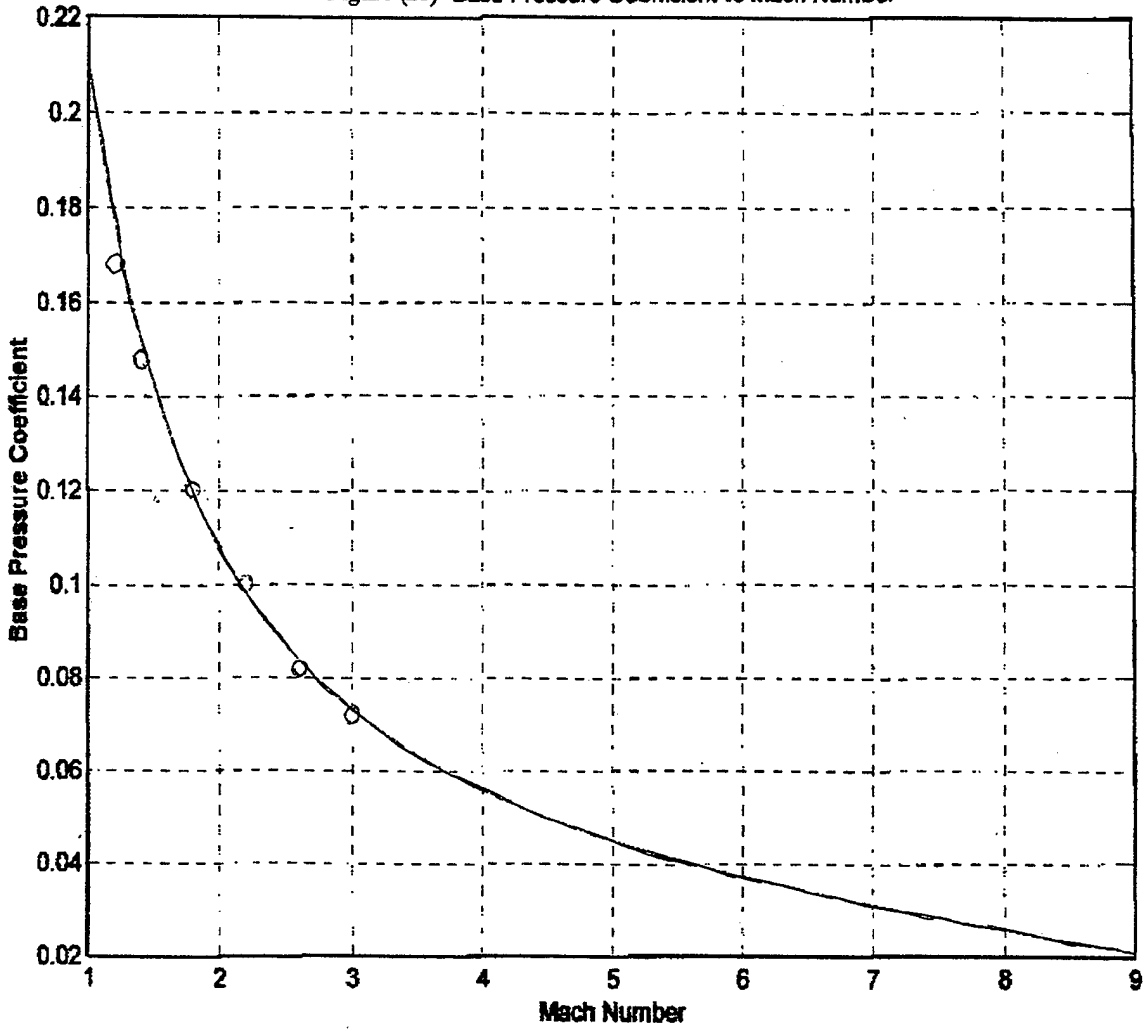

LIST OF REFERENCES

1. Chin, S.S., *Missile Configuration Design*, McGraw-Hill Book Company, Inc., 1961.

2. Pitts, W. C., Nielsen, J. N., and Kaattari, G. E., *Lift and Center of Pressure of Wing-Body-Tail Combinations at Subsonic, Transsonic, and Supersonic Speeds*, NACA Report 1307.

3. Kemp, N. H. and Riddell, F. R., "Heat Transfer to Satellite Vehicles Re-entering the Atmosphere," *Jet Propulsion*, vol. 27, no. 2, part 1, p. 137, February 1957.

4. Zucker, R. D., *Fundamentals of Gas Dynamics*, Matrix Publishers, Inc., 1977.

5. Hoak, D. E. and Finck, R. D., *U.S. Air Force Stability and Control DATCOM Vol.3 Sec. 5*, Engineering Documents, 1960.

6. Blackadar, A. K., "Wind," *Microsoft Encarta 97 Encyclopedia*, Microsoft Corporation, 1996.

7. Anderson, J. D. Jr., *Introduction to Flight*, McGraw-Hill Book Company, Inc., 1979.

INITIAL DISTRIBUTION LIST

1. Defense Technical Information Center 2
   8725 John J. Kingman Road, STE 0944
   Ft. Belvoir, Virginia 22060-6218

2. Dudley Knox Library 2
   Naval Postgraduate School
   411 Dyer Rd.
   Monterey, California 93943-5101

3. Engineering & Technology Curricular Office (Code 34) 1
   Naval Postgraduate School
   Code 34
   700 Dyer Road, Bldg 245 Rm 115
   Monterey, California 93943-5109

4. Professor Conrad F. Newberry 2
   AA/Ne
   Department of Aeronautics and Astronautics
   Naval Postgraduate School
   Monterey, California 93943-5106

5. Professor William B Maier, II 2
   Department of Physics
   Naval Postgraduate School
   Monterey, California 93943

6. LCDR Francisco M. Juanche 1
   1050 Camino Atajo
   Chula Vista, California